Lack of collagen XVIII leads to lipodystrophy and perturbs hepatic glucose and lipid homeostasis

Tiina Petäistö[1], David Vicente[1], Kari A. Mäkelä[2], Mikko A. Finnilä[3], Ilkka Miinalainen[4], Jarkko Koivunen[1] (iD), Valerio Izzi[1] (iD), Mari Aikio[1], Sanna-Maria Karppinen[1], Raman Devarajan[1] (iD), Jerome Thevenot[3], Karl-Heinz Herzig[2] (iD), Ritva Heljasvaara[1,5] and Taina Pihlajaniemi[1] (iD)

[1]*Oulu Center for Cell-Matrix Research, Faculty of Biochemistry and Molecular Medicine, University of Oulu, Oulu, Finland*
[2]*Research Unit of Biomedicine, Biocenter Oulu and Faculty of Medicine, University of Oulu, Oulu, Finland*
[3]*Research Unit of Medical Imaging, Physics and Technology, Faculty of Medicine, University of Oulu, Oulu, Finland*
[4]*Biocenter Oulu, University of Oulu, Oulu, Finland*
[5]*Department of Biomedicine, Centre for Cancer Biomarkers (CCBIO), University of Bergen, Bergen, Norway*

Edited by: Kim Barrett & Bettina Mittendorfer

Linked articles: This article is highlighted in a Perspectives article by Bonaldo & Cescon and a Journal Club article by Braun et al. To read these articles, visit https://doi.org/10.1113/JP280226 and https://doi.org/10.1113/JP279877.

Key points

- Extracellular matrix is highly remodelled in obesity and associates with the development of metabolic disorders, such as insulin resistance.
- Previously, we have shown that the lack of specific collagen XVIII isoforms impairs adipocyte differentiation in mice.
- Here, we show that mice lacking the medium and long isoforms of collagen XVIII develop insulin resistance and glucose intolerance and show elevated serum triglycerides and fat accumulation in the liver.
- We report that collagen XVIII-deficient mice have increased heat production at low temperatures.
- These results reveal a new role for collagen XVIII in the regulation of glucose and lipid metabolism, and they expand the understanding of the development of metabolic disorders.

Abstract Liver and adipose tissues play important roles in the regulation of systemic glucose and lipid metabolism. Extracellular matrix synthesis and remodelling are significantly altered in these tissues in obesity and type 2 diabetes. Collagen XVIII is a ubiquitous extracellular matrix component, and it occurs in three isoforms which differ in terms of molecular size, domain structure and tissue distribution. We recently showed that, in mice, the lack of collagen XVIII, and especially its medium and long isoforms, leads to reduced adiposity and dyslipidaemia. To address the metabolic consequences of these intriguing observations, we assessed whole-body glucose homeostasis in mice challenged with a high-fat diet and in normal physiological conditions.

Tiina Petäistö got her MSc in Molecular and Cellular Biology in 2014 at the University of Oulu (Finland). Currently she is doing her PhD in the same university, pursuing the roles of the extracellular matrix protein collagen XVIII in metabolism and adipose tissue development. She has also expertise in studying the collagens in skin homeostasis. **David Vicente** is a veterinary surgeon specialist in small animal orthopaedics and soft tissue surgery. He completed his PhD in Biomedical Sciences in 2014 at the University of Oulu (Finland). His PhD thesis addressed the role of collagen XVIII in lipid and glucose metabolism and collagen XV in bone development. His main areas of research include canine and feline orthopaedic and oncological diseases.

T. Petäistö and D. Vicente contributed equally to this work.

We observed that, in the high caloric diet, the overall adiposity was decreased by 30%, serum triglyceride values were threefold higher and the steatotic area in liver was twofold larger in collagen XVIII knockout mice compared with controls. We demonstrated that mice lacking either all three collagen XVIII isoforms, or specifically, the medium and long isoforms develop insulin resistance and glucose intolerance. Furthermore, we found that ablation of collagen XVIII leads to increased heat production in low temperatures and to reduction of the high blood triglyceride levels of the knockout mice to the level of wild-type mice. Our data indicate that collagen XVIII plays a role in the regulation of glucose tolerance, insulin sensitivity and lipid homeostasis, principally through its ability to regulate the expansion of the adipose tissue. These findings advance the understanding of metabolic disorders.

Corresponding author T. Pihlajaniemi: Oulu Centre for Cell-Matrix Research, Faculty of Biochemistry and Molecular Medicine, University of Oulu, PO Box 5400, FI-90014 University of Oulu, Oulu, Finland.   Email: taina.pihlajaniemi@oulu.fi

Introduction

Overweight and obesity cause serious health problems worldwide, and the proportion of overweight people is continually increasing (World Health Organization, 2017). Obesity is frequently associated with insulin resistance, which in turn is linked to the development of type 2 diabetes, hypertension, hyperlipidaemia – the so-called metabolic syndrome – and atherosclerosis (Hanson *et al.* 2002; Wilson *et al.* 2005). Another spectrum of adipose tissue dysfunction is lipodystrophy, which is characterized by severe deficiency in adipose tissue mass and associates with a similar metabolic phenotype seen in obesity (Mann & Savage, 2019).

White adipose tissue (WAT) is a primary site for energy storage but also a major factor in the regulation of metabolic functions (Rosen & Xu, 2009). Impaired energy storage in the WAT, for example, in the case of lipodystrophy, often causes ectopic lipid accumulation in the liver and high triglyceride (TG) levels in blood (Asterholm *et al.* 2007). Brown adipose tissue (BAT) is functionally distinct from WAT. Instead of storing energy, BAT consumes fatty acids and can produce heat in order to maintain body temperature. Cold exposure is one of the most effective thermogenic stimulators and activates mitochondria to produce heat through a brown adipocyte-specific protein, uncoupling protein 1 (UCP1) (Carobbio *et al.* 2019), and induces TG clearance from the blood by increasing fatty acid uptake into BAT in conditions such as lipodystrophy (Bartelt *et al.* 2011). Beige adipocytes are located within the WAT and have brown-like characteristics, such as expression of UCP1. Browning of WAT and the activation of beige/brown adipocytes are topical issues in metabolic research for their therapeutic potential against obesity and metabolic disorders (Montanari *et al.* 2017).

Adipocytes secrete numerous extracellular matrix (ECM) proteins that provide structural support to the tissue (Mariman & Wang, 2010). Our recent work has shed light on the functional relevance of the collagen family of ECM proteins in adipose tissues. We found that collagen XVIII, a ubiquitous basement membrane component, promotes adipose tissue accrual by influencing the number of adipocyte progenitor cells in epididymal white adipose tissue (eWAT). In humans, mutations in *COL18A1* lead to Knobloch syndrome, a rare condition characterized mainly by ocular and skull defects (Caglayan *et al.* 2014; Heljasvaara *et al.* 2017). In addition, a *COL18A1* c.1136C>T variant has been shown to associate with obesity in type 2 diabetes patients, and a c.331G>A variant has a large effect on serum TG level (Errera *et al.* 2008; Peloso *et al.* 2014). Mice lacking collagen XVIII have increased serum TG levels, and similarly, Knobloch patients are shown to suffer from hyper-triglyceridaemia, albeit the effects on body mass or adipose tissue are not known (Bishop *et al.* 2010; Aikio *et al.* 2014). Additionally, collagen XVIII deficiency increases atherosclerosis in mice (Moulton *et al.* 2004). Collagen XVIII is expressed as three isoforms which differ in terms of molecular size, amino-terminal domain structure and tissue distribution. These isoforms originate from the use of two gene promoters (P) and alternative mRNA splicing of the longest transcript (Heljasvaara *et al.* 2017). The short isoform, present in most tissues in association with vascular and epithelial basement membranes, derives from the P1-controlled transcript. Medium and long iso-forms are abundant in the basement membranes in liver and WAT and are generated by a downstream P2 and alternative splicing of exon 3. The two longer variants share a mucin-like domain (MUCL-C18) in the N-terminus (Kaur *et al.* 2018) followed by a thrombospondin 1-like domain (TSP-1), which is also found in the N-terminus of the short variant. The longest isoform has an additional frizzled domain homologous to the extracellular part of the Wnt-binding frizzled receptors (Rehn & Pihlajaniemi, 1995). The highest expression of collagen XVIII is detected

in liver and this is largely attributed to the occurrence of the medium isoform in the perisinusoidal spaces (Rehn & Pihlajaniemi, 1995; Musso *et al.* 1998; Saarela *et al.* 1998). In addition, fat tissue contains relatively high amounts of collagen XVIII, surrounding adipocytes and blood vessels, and its expression level increases during adipocyte differentiation (Inoue-Murayama *et al.* 2000; Aikio *et al.* 2014).

We have previously shown that collagen XVIII regulates adipogenesis specifically via the medium/long isoforms, and the lack of these isoforms in mice leads to reduced adiposity and predisposes to fat accumulation in the liver (Aikio *et al.* 2014). Considering that liver and fat tissues are the key regulators of glucose and lipid metabolism, we investigated here how collagen XVIII affects glucose metabolism and lipid homeostasis in obese mice with metabolic dysfunction and in lean mice without metabolic challenging. Mice lacking all three collagen XVIII isoforms ($Col18a1^{-/-}$), as well as P1 ($Col18a1^{P1/P1}$) and P2 ($Col18a1^{P2/P2}$)-specific knockout (KO) mouse lines (Fukai *et al.* 2002; Aikio *et al.* 2014), were subjected to either a high-fat diet (HFD) or standard chow, and metabolic parameters and glucose metabolism were evaluated. Additionally, the role of collagen XVIII in energy metabolism was investigated by activating non-shivering thermogenesis in the BAT by cold exposure, and metabolic parameters were measured. We found that lack of collagen XVIII predisposed mice to metabolic dysfunctions, more specifically to abnormal lipid accumulation in liver combined with impaired insulin sensitivity and glucose tolerance. Collagen XVIII deficiency also affected energy metabolism by increasing the heat production, and cold exposure lowered the abnormally high serum TG levels in the mutant mice to the same level as that of the wild-type (WT) mice. Our results suggest a novel role for collagen XVIII in the regulation of glucose homeostasis and insulin sensitivity as a result of ectopic lipid accumulation. Additionally, our data provide new information on the roles of the ECM in the complex development of metabolic disorders.

Methods

Ethical approval

All animal experiments were approved by the Laboratory Animal Centre of the University of Oulu or the Animal Board of the State Provincial Office of Southern Finland (permissions ESAVI-973-04.10.03-2012, ESAVI-3896-04.10.03-2012, ESAVI-7572-04.10.03-2012, ESAVI/6105/04.10.07/2015 and ESAVI/24 668/2018). Mice were maintained on a 12 h light–12 h dark cycle, and they had free access to tap water and were fed *ad libitum.* Prior to the experiments, all mice were fed a standard rodent chow diet containing approximately 5% (w/w) fat

(Teklad Global Rodent diet, T.2018C.12; Harlan Teklad, USA). Mice had aspen chips as bedding material, nesting box and aspen shavings for nesting material and a cube tunnel as an enrichment. Mice were euthanized by CO_2 inhalation followed by cervical dislocation.

Animals

Generation of the collagen XVIII-deficient ($Col18a1^{-/-}$), promoter 1- ($Col18a1^{P1/P1}$) and 2- ($Col18a1^{P2/P2}$) specific KO mouse lines was described earlier (Fukai *et al.* 2002; Aikio *et al.* 2014). For the metabolic studies, male mice at 4–10 weeks of age were fed either a normal diet containing either 5% (w/w) fat or a high-fat diet containing 0.2% cholesterol and 21% (w/w) fat (TD.88137; Harlan Teklad, Envigo, Indianapolis, IN, USA) for 20 weeks. During this period, mouse body weight was registered on a weekly basis for 12 weeks. Linear regression analysis was performed to exclude the potential effect of the age on fat accrual (data not shown). Glucose and insulin baseline values were also measured in unchallenged female mice, but as there were no differences between the sexes, further tolerance tests were performed only with male mice. Cold exposures were performed for male mice at 14–15 weeks of age on a standard chow. Noradrenaline (NA) stimulations were performed with 12-week-old male mice on a standard chow.

Calorimetry and metabolic performance

Metabolic and behavioural home cage analyses of food and water intake, physical activity (number of infrared beam breaks), O_2 consumption and CO_2 production of male mice fed for 12–18 weeks on a HFD ($Col18a1^{-/-}$ ($n = 11$), $Col18a1^{P1/P1}$ ($n = 7$), $Col18a1^{P2/P2}$ ($n = 8$), and WT ($n = 11$)) were performed using an automated analysing system (TSE Systems GmbH, Bad Homburg, Germany). Due to the limited number of metabolic cages, the different genotypes were divided into randomized groups for measurements. Hence, some mice consumed HFD for a longer time before the metabolic parameters were obtained; however, the HFD consumption times did not have significant effects on the results (Fig. 1). Before the measurements, the mice were accommodated in individual training cages for 7 days. After transfer to the analysis cages, the mice were adapted for 48 h before starting the measurements. All the cages were equipped with wooden chips as bedding. Data were collected for 114 h (measurement started at 09.00 h) at room temperature ($21 \pm 1°C$, air humidity 40–60%).

Cold exposure

Cold exposure experiments were performed in two series with 14- to 15-week-old male mice as follows:

$Col18a1^{-/-}$ + WT mice ($n = 3 + 3$) and $Col18a1^{P2/P2}$ + WT mice ($n = 4 + 4$). The mice were fed standard chow and housed individually in cages over the entire time of the experiment. After 7 days adaptation to the training cages in room temperature, the mice were housed in the metabolic cages (described above) at 18°C for 7 days (cold adaptation), followed by cold exposure (4°C) for 7 days. Gas exchange, physical activity and food consumption were recorded during the cold adaptation and exposure. Heat production was calculated by applying the abbreviated Weir equation [$H = (3.94 \times \dot{V}_{O_2}) + (1.1 \times \dot{V}_{CO_2})$] (Weir, 1949) and normalized to the body weight.

Whole-body micro-computed tomography scan and fat volume measurement

Whole-body micro-computed tomography (μCT) (SkyScan 1076; Bruker MicroCT, Kontich, Belgium) was performed to assess the body composition by quantifying
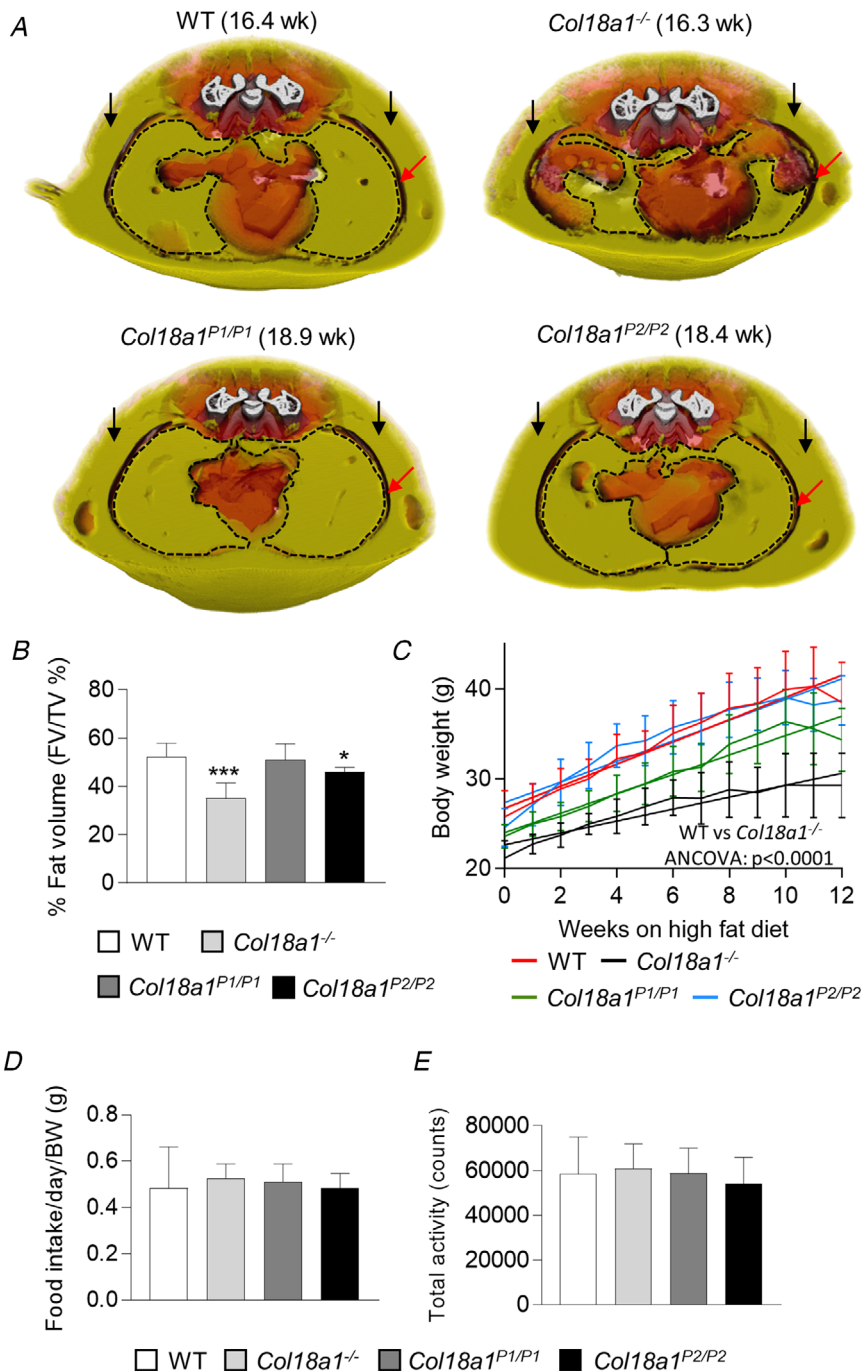

Figure 1. Loss of collagen XVIII leads to a decreased WAT volume and retards the body weight gain of $Col18a1^{-/-}$ mice on a HFD

A, representative μCT images showing the adipose tissue at the level of lumbar vertebra L6 in male mice at the indicated ages, fed on a HFD for 10 weeks. Adipose tissue is presented as yellow, other soft tissues as red and bone as white. Intra-abdominal adipose tissue is surrounded with black dashed lines and black arrows indicate subcutaneous adipose tissue. Red arrows indicate the abdominal muscle layer separating the visceral and subcutaneous adipose tissues. *B*, proportions of fat volume per total body volume (FV/TV%) in abdominal regions (L1–S1) of the specified mouse lines fed with a HFD for 10 weeks. FV and TV were obtained through μCT image analysis (means ± SD). *C*, weekly body weights of WT and *Col18a1* mutant mice fed with a HFD for 12 weeks (means + SD). *D* and *E*, food intake (*D*) and physical activity (*E*) (the number of infrared beam breaks) of the HFD-fed mice during the 114 h metabolic cage study (means + SD). In *A–E*: WT, $n = 11$; $Col18a1^{-/-}$, $n = 6$; $Col18a1^{P1/P1}$, $n = 7$; and $Col18a1^{P2/P2}$, $n = 8$. Statistical significance was tested by one-way ANOVA with Benjamini–Kieger–Yekutieli false discovery rate or linear regression analysis ANCOVA; *$P < 0.05$, ***$p < 0.001$. [Colour figure can be viewed at wileyonlinelibrary.com]

relative volumes of adipose tissues. Male mice on the HFD for 10 weeks were imaged in a supine position on the radiolucent bed. Anaesthesia was provided with 1–2% isoflurane carried by O_2 through a nose cone during the scan. The μCT X-ray tube was set to 50 kV with 476 μA, and projection images with isotropic voxel size of 35 μm were collected every 0.6° over 360° rotation with a 70 ms exposure time and frame averaging of 3. Images were reconstructed with corrections for beam hardening and ring artefact with NRecon v 1.7.1 software (Bruker MicroCT). The adipose tissue volume fraction relative to the body volume was measured for the abdominal regions extending from the first lumbar vertebra (L1) to the proximal processes of the first sacral (S1) vertebra. Fat tissues were segmented from 3D image stacks by applying low and high pass thresholds with CTAn v1.17.7.2 software (Bruker MicroCT). Quantified tissue volumes were compared against total body volume in the segment, providing fat volume fraction (%). The number of mice analysed was as follows: WT, $n = 11$; $Col18a1^{-/-}$, $n = 6$; $Col18a1^{P1/P1}$, $n = 6$; and $Col18a1^{P2/P2}$, $n = 8$.

In vivo lipolysis analysis

The ability of adipose tissue to respond to β-adrenergic stimulation was assessed in WT and $Col18a1^{-/-}$ mice ($n = 3 + 3$) at the age of 12 weeks. The mice were fasted 24 h before the experiment and anaesthetized with a subcutaneous (s.c.) injection of fentanyl–midazolam–medetomidine mixture. An initial blood sample (0 min) was collected from the tail vein after which the lipolysis was stimulated with NA (1 mg kg^{-1} s.c.; cat. no. 74480, Sigma-Aldrich, St Louis, MO, USA) for 35 min. A blood sample was collected from the vena cava at the end of the experiment. Rectal body temperature was followed during the experiment and recorded every 2 min.

Preadipocyte isolation, differentiation and lipolysis assay *in vitro*

Lipolysis was analysed *in vitro* with differentiated preadipocytes. Preadipocytes were isolated from the inguinal fat depots from 6-week-old male mice and the depots from four to five mice were pooled together. Adipose tissue was minced thoroughly and digested with 2.5 mg ml^{-1} collagenase D (cat. no. 11088866001, Roche, Basel, Switzerland), 3.1 U ml^{-1} dispase II (cat. no. D4693, Sigma-Aldrich) and 10 mM CaCl$_2$ for 45 min at 37°C, and shaken regularly during the digestion. After that, collagenase activity was inhibited with the complete preadipocyte medium consisting of DMEM/F12 (cat. no. 10565018, Thermo Fisher Scientific, Waltham, MA, USA), supplemented with 10% FBS

(S1810-500, Biowest, Nuaillé, France), 0.1 mg ml^{-1} Primocin (Primocin anti-pm-2, InvivoGen, San Diego, CA, USA), 1 × penicillin–streptomycin (cat. no. P0781, Sigma-Aldrich). The tissue suspension was filtered through a 70 μm Cell Strainer (cat. no. 352350, Corning, Corning, NY, USA) and the stromal vascular fraction was pelleted by centrifugation 5 min, 600 g. The pellet was resuspended in the complete preadipocyte medium and filtered through 40 μm Cell Strainer (cat. no. 352340, Corning). The cells were centrifuged and plated in complete preadipocyte medium. Next day, the cells were washed four times with 1 × phosphate-buffered saline and medium was changed every day until the cells reached 90% confluence. For adipocyte differentiation, isolated preadipocytes were grown to confluence and 2 days post-confluence the medium was supplemented with 5 μg ml^{-1} insulin (cat. no. I6634, Sigma-Aldrich), 1 μM rosiglitazone (cat. no. 71740, Cayman Chemical Co., Ann Arbor, MI, USA), 0.5 mM IBMX (cat. no. I7018, Sigma-Aldrich) and 1 μM dexamethasone (cat. no. D4902, Sigma-Aldrich) for 2 days and the medium was changed every day. From day 2 onwards the medium was supplemented only with insulin and rosiglitazone until day 6. On day 6 the differentiated cells were treated with 10 μM NA and cell medium was collected at 0, 3 and 6 h time points. The amount of glycerol released to the medium was measured with a glycerol assay kit (cat. no. MAK117, Sigma-Aldrich) according to the manufacturer's instructions. The experiment was performed with three cell lines per genotype ($n = 3$ per genotype).

Determination of serum lipids

The male mice on a HFD for 20 weeks were fasted for 3 h and blood was drawn via the saphenous vein. Serum total cholesterol and TGs were measured by enzymatic colorimetric methods (Makela *et al.* 2008). After the chronic cold exposure, the mice were not fasted, and blood samples were collected via the vena cava. The cholesterol and TG levels were analysed in the Nordlab clinical service laboratory (Oulu University Hospital, Finland) and free fatty acid (FFA) concentrations were measured by the Free Fatty Acid Assay Kit – Quantification (cat. no. ab65341, Abcam, Cambridge, UK) according to the manufacturer's instructions. The number of analysed serum samples from mice on HFD was $n = 4$ for each of the four genotypes, after the chronic cold exposure, $Col18a1^{-/-}$ + WT mice ($n = 3 + 3$) and $Col18a1^{P2/P2}$ + WT mice ($n = 4 + 4$), and in the NA stimulation experiment, $Col18a1^{-/-}$ + WT mice ($n = 3 + 3$).

Histology

Liver, eWAT, inguinal WAT (iWAT) and interscapular BAT samples were fixed in 4% paraformaldehyde, embedded

in paraffin, cut into 5 μm-thick sections and stained with hematoxylin–eosin (H&E) in order to characterize histological changes in the samples. Steatotic area was measured by thresholding the picture into two phases with ImageJ software (NIH, Bethesda, MD, USA), and two to three images per sample were analysed. Oil Red O staining was performed for snap-frozen liver samples. Samples were embedded in Tissue-Tek OCT Compound (Sakura Finetechnical, Tokyo, Japan), cut into 5 μm-thick sections and fixed with 10% formalin. Sections were visualized under a Zeiss Axio Imager microscope (jena, Germany). The number of liver samples analysed was as follows: WT, $n = 7$; $Col18a1^{-/-}$, $n = 6$; $Col18a1^{P1/P1}$, $n = 6$; and $Col18a1^{P2/P2}$, $n = 8$; and other tissues, $n = 3$–4 per genotype.

Immunohistochemistry

Paraffin-embedded BAT and WAT samples were stained against UCP1 antibody (cat. no. U6382, 1:500; Sigma-Aldrich) using the HistoMouse kit (Thermo Fisher Scientific) according to the manufacturer's instructions. Staining was imaged by a Zeiss Axio Imager microscope. The number of samples analysed was three to four per genotype.

Electron microscopy

BAT samples from mice housed at room temperature and after cold exposure were fixed in 1% glutaraldehyde, 4% formaldehyde in 0.1 M phosphate buffer (pH 7.4), post-fixed with osmium tetroxide, dehydrated in acetone and embedded in Epon LX 112 (Ladd Research Industries, Williston, VT, USA). Ultrathin sections (70 nm) were cut with a Leica UC6 ultramicrotome (Leica Microsystems, Wetzlar, Germany), post-stained in uranyl acetate and lead citrate and imaged with a Tecnai G2 Spirit transmission electron microscope (FEI Europe, Eindhoven, The Netherlands) using a Quemesa CCD camera (Olympus Soft Imaging Solutions GmbH, Münster, Germany). The amount of cytoplasm was measured by thresholding the picture into two phases, lipid droplets and cytoplasm, with ImageJ software. Numbers of samples analysed were three to four per genotype and three to five images were analysed per sample.

Real-time quantitative PCR

Total RNA from snap-frozen tissues from male mice on a HFD for 20 weeks or after cold exposure were isolated for real-time quantitative PCR (RT-qPCR) analyses using TRIzol Reagent (Thermo Fisher Scientific). The cDNA was synthesized from 1 μg of total RNA using the iScript cDNA Synthesis Kit (Bio-Rad Laboratories, Hercules, CA, USA)

Table 1. Primers sequences used in real-time quantitative PCR

Gene	Forward primer (5′ to3′)	Reverse primer (5′ to 3′)
Adipoq	CCGGAACCCCTGGCAG	CTGAACGCTGAGCGATACACA
Cidea	GCAGGAACTTATCAGCAAGA	CGTAACCAGGCCAGTTGTGAT
Cox7a1	CAGCGTCATGGTCAGTCTGT	AGAAAACCGTGTGGCAGAGA
Dio2	AATTATGCCTCGGAGAAGACCG	GGCAGTTGCCTAGTGAAAGGT
Gapdh	ACCACAGTCCATGCCATCAC	TCCACCACCCTGTTGCTGTA
Glut2	ACGGATGCCAATTACCGACA	TGCTGGGCCATGTGCA
Glut4	ATGAGAAACGGAAGTTGGAGAGA	GTGGGTGCGGCTGCC
G6PC	AAGCCAACGTATGGATTCCG	ACAGCAATGCCTGACAAGACT
Klf15	CACCAAGAGCAGCCACCTCA	CGGGACACTGGTACGGCTTC
Nd1	CTAGCAGAAACAAACCGGGC	CCGGCTGCGTATTCTACGTT
Pgc-1α	CATTTGATGCACTGACAGATGGA	GTCAGGCATGGAGGAAGGAC
Pparα	GACAAGGCCTCAGGGTACCA	GCCGAATAGTTGCCGAAA
PPIA	GAGCTGTTTGCAGACAAAGTTC	CCCTGGCACATGAATCCTGG
Sln	GCACTAGGTCCTTGGCATGT	ACTCAAGGGACTGGCAGAGA
Serca 1/2	GACGAGTTTGGGGAGCAGCT	AGGTGGTGATGACAGCAGG
Ucp1	CGACTCAGTCCAAGAGTACTCTCTTC	GCCGGCTGAGATCTTGTTTC

following the manufacturer's instructions. RT-qPCR was performed using iTaq Universal SYBR Green (Bio-Rad) in a CFX96 Touch Real-Time PCR Detection System (Bio-Rad). Relative RNA levels were calculated using the $2^{-\Delta\Delta C_T}$ method. Values were normalized to *β-actin*, *18S rRNA* or *PPIA* (peptidylprolyl isomerase A). The amount of mitochondrial DNA (mtDNA) was assessed by measuring the mitochondrial gene NADH dehydrogenase subunit 1 (*Nd1*), and normalized to the nuclear gene *PPIA*. Primer sequences are listed in Table 1. The number of samples analysed was three to eight per genotype.

Alanine aminotransferase and aspartate aminotransferase analysis

Liver function was tested in male mice on a HFD for 20 weeks by measuring the levels of common hepatic damage markers, alanine aminotransferase (ALT) and aspartate aminotransferase (AST), in serum samples.

Analysis was conducted in the NordLab clinical service laboratory (Oulu University Hospital, Finland). The number of samples analysed was $n = 6$ per genotype.

Glucose tolerance test

Glucose tolerance was studied in male mice on a HFD for 12 weeks and on a normal chow. Glucose tolerance tests (GTTs) were performed by fasting the mice overnight for 16 h followed by intra peritoneal (I.P.) injection of 2 g kg^{-1} glucose (Sigma-Aldrich) in phosphate-buffered saline as previously described (Lamming *et al.* 2012). Blood was drawn via the saphenous vein before injection and at 15, 30, 60 and 90 min after the injection and was assayed for glucose using a Bayer Contour blood glucose meter. Blood samples were centrifuged at 5400 *g* for 10 min at 4 °C, and plasma was collected and kept at −80°C until analysis. The number of analysed plasma samples from animals fed with HFD was: WT, $n = 11$; *Col18a1$^{-/-}$*, $n = 6$; *Col18a1$^{P1/P2}$*, $n = 6$; and *Col18a1$^{P2/P2}$*, $n = 8$; and from those on a normal chow, $n = 6$ per genotype.

Plasma adiponectin and insulin measurements

The plasma adiponectin and insulin concentrations were determined by a colorimetric sandwich enzyme-linked immunosorbent assays (ELISA) using a R&D Quantikine mouse adiponectin immunoassay kit (R&D Systems, Minneapolis, MN, USA) and an Ultrasensitive Mouse Insulin ELISA kit (Crystal Chem Inc., Elk Grove Village, IL, USA), respectively. Determinations were done in duplicate following the manufacturer's instructions. The number of samples analysed was $n = 5$–10 per genotype.

Hyperinsulinaemic–euglycaemic clamp studies

Hyperinsulinaemic–euglycaemic clamps (insulin clamps) were performed with 26-week-old male mice as described (Nakamura *et al.* 2014). Briefly, 4 days before the clamp experiments, the right jugular vein of each mouse was catheterized with a polyethylene tube filled with heparin solution (100 units ml^{-1}). After 16 h fasting, a 135 min insulin clamp procedure was conducted with a primed-continuous infusion of human insulin (Novolin; Novo Nordisk, Denmark) at a rate of 12.5 mU kg^{-1} min^{-1}. Blood samples were collected from incisions in the tail at 3–20 min intervals for the immediate measurement of blood glucose concentration, using a Bayer Contour blood glucose meter; 25% glucose was infused at variable rates to maintain plasma glucose at basal concentrations. To estimate insulin-stimulated glucose uptake in tissues, 2-[^{14}C]deoxyglucose (Perkin Elmer, Inc., Waltham, MA, USA) was administered as a bolus (0.6 µCi g^{-1}) 75 min after the start of clamping. Afterwards, for the determination of blood 2-[^{14}C]deoxyglucose concentrations, blood samples (100 µl) were collected at different time points during 1 h. At the end, 50 mg of liver, eWAT, soleus muscle and 100 µl blood samples were homogenized in 1:1 or, in the case of eWAT, 2:1 chloroform–methanol and centrifuged. The pellet was re-extracted in a chloroform–methanol solution and centrifuged again. The supernatants were scintillated for ^{14}C activity by a Perkin Elmer Liquid Scintillation Analyzer (Tri-Carb 2900TR). The results are presented as counts per minute (cpm) per 50 mg of tissue. The number of animals in the experiment was $n = 6$ per genotype.

Statistical analysis

Data in figures and tables are presented as means ± SD. Overall probability values for genotype differences were based on Student's unpaired *t* test, one-way or two-way ANOVA with Benjamini–Kieger–Yekutieli false discovery rate or ANCOVA, and $P \leq 0.05$ was considered statistically significant.

Results

Collagen XVIII deficiency regulates body weight gain and fat accrual on a long-term HFD

In a previous study, we demonstrated that both the *Col18a1$^{-/-}$* mice, totally lacking collagen XVIII expression, and the *Col18a1$^{P2/P2}$* mice, lacking exclusively the medium/long isoforms, have smaller eWAT depots due to impaired adipogenesis (Aikio *et al.* 2014). This reduced adiposity was detected in animals fed with a standard chow or a short-term (5 weeks) HFD, containing 5% and 21% fat, respectively, and was associated with ectopic fat accumulation in the liver. To uncover the metabolic consequences of collagen XVIII ablation during long-term consumption of a HFD, the WT, *Col18a1$^{-/-}$*, *Col18a1$^{P1/P1}$* (lacking exclusively the short collagen XVIII isoform) and *Col18a1$^{P2/P2}$* mice were fed with high caloric chow for 20 weeks. The extent of intra-abdominal and subcutaneous adipose tissue in the mice after 10 weeks on the HFD was assessed by μCT. The adipose tissue volume fraction relative to the body volume was measured for the abdominal regions extending from L1 to the proximal processes of the first sacral vertebra. Representative images of tissue segmentations at the level of L6 revealed clearly reduced amounts of subcutaneous and visceral adipose tissues in the *Col18a1$^{-/-}$* mice compared to the WT mice (Fig. 1*A*). Moreover, μCT software analysis demonstrated that the proportion of adipose tissue volume in the abdominal region was significantly reduced both in the *Col18a1$^{-/-}$* and in the *Col18a1$^{P2/P2}$* mice, but not in the *Col18a1$^{P1/P1}$* mice (Fig. 1*B*).

The body weight gain of the $Col18a1^{-/-}$ mice on the HFD was significantly slower than that of the WT, whereas the body weight gain of the $Col18a1^{P1/P1}$ and $Col18a1^{P2/P2}$ mice did not differ from that of the WT (Fig. 1C), tested with the ANCOVA linear regression analysis method. Food intake and physical activity were analysed in all mouse lines on the HFD using an automated monitoring system. The mice were placed in the home cages and adapted for one week and cumulative recordings were collected over the following 114 h. No differences were observed in activity and food consumption (Fig. 1D and E). These data confirm that the decreased fat volume in the collagen XVIII-deficient mice is not derived from differential physical activity or food consumption.

Lack of collagen XVIII affects the lipid profiles in the blood and liver

Lipodystrophy often predisposes to dyslipidaemia, which is mainly characterized by severe hypertriglyceridaemia in the blood (Akinci *et al.* 2018). In order to understand the involvement of collagen XVIII in blood lipid metabolism, we measured fasting cholesterol and TG levels in the serum of the mice fed with a long-term HFD. Previously, we have shown a 30% increase in serum TG levels in the $Col18a1^{P2/P2}$ mice compared to WT mice after 5 weeks on the HFD, whereas the $Col18a1^{-/-}$ and $Col18a1^{P1/P1}$ mice showed no differences in their blood lipid levels (Aikio *et al.* 2014). Twenty weeks of HFD feeding provoked significant differences in serum TG levels of mice lacking either all or the medium and long collagen XVIII iso-forms, revealing a remarkable increase of approximately 200% in the $Col18a1^{-/-}$ mice and a 75% increase in the $Col18a1^{P2/P2}$ mice compared with the WT mice, whereas in the $Col18a1^{P1/P1}$ mice, which lack only the short iso-form, the serum TG levels equalled those of the WT mice (Fig. 2A). Cholesterol levels were not altered amongst the genotypes either (Fig. 2B).

After long-term HFD feeding, fat accumulated in the livers of the WT and mutant mice. The mutant mice showed a significantly higher steatotic area in the livers compared with the WT mice (Fig. 2C). Severe histological changes were observed in the livers of the $Col18a1^{-/-}$ and the $Col18a1^{P2/P2}$ mice compared to the livers of the WT mice, including both micro- and macrovesicular steatosis (Fig. 2D, H and E staining). Compared with WT mice, the $Col18a1^{P1/P1}$ mice showed higher fatty degeneration, but to a lesser extent than the $Col18a1^{-/-}$ and $Col18a1^{P2/P2}$ mice (Fig. 2C and D). All genotypes included both micro- and macrovesicular steatosis distributed evenly in the livers. However, macrovesicular steatosis was more prominent in the mutant mice compared with the control mice. Fat depositions were also observed in all genotypes by Oil Red O staining (Fig. 2D). However, the WT mice had clearly smaller lipid droplets than the other genotypes, indicative of microvesicular steatosis, and this could be detected both in H&E and in Oil Red O staining. Furthermore, the liver weight to body weight ratio was significantly increased in the $Col18a1^{-/-}$ and the $Col18a1^{P2/P2}$ mice fed with the HFD, but not in the $Col18a1^{P1/P1}$ mice, as compared with the WT mice on the same diet (Fig. 2E).

Hepatic damage was also evident in the $Col18a1^{-/-}$ and $Col18a1^{P2/P2}$ mice in liver function tests. An increased level of serum ALT is an indicator of hepatic damage (Xu *et al.* 2003), and AST is associated with damage to the liver, as well as other organs (Fontana & Lok, 2002). The ALT and AST levels were 3- and 1.6-fold higher, respectively, in the serum of $Col18a1^{P2/P2}$ mice compared with WT mice (Fig. 2F and G). The $Col18a1^{-/-}$ mice had a twofold increase in serum ALT levels, while AST levels were normal, and the $Col18a1^{P1/P1}$ mice showed no changes in these markers (Fig. 2F and G). Taken together, our previous data and the present liver and blood analyses indicate that impaired adipogenesis in the mice lacking specific collagen XVIII isoforms leads to the ectopic lipid accumulation in blood and liver and causes liver damage.

Glucose and lipid homeostasis in *Col18a1* mutant mice on HFD

To explore the physiological effects of the apparent adipose tissue dysfunction in the absence of collagen XVIII, we first quantified protein and transcript levels of selected key genes involved in glucose and lipid homeostasis in the mutant *Col18a1* mice and in controls fed for 20 weeks with a HFD. The circulating levels of adiponectin, an abundant adipose tissue-derived hormone critical for whole-body glucose homeostasis (Rosen & Spiegelman, 2006), were decreased in the $Col18a1^{-/-}$ mice by 26% and in the $Col18a1^{P2/P2}$ mice by 37% compared with the WT mice (Fig. 3A). The serum adiponectin level was slightly decreased, by 15%, in the $Col18a1^{P1/P1}$ mice, too, even though their adipose tissue volume was not decreased. Compared with the WT mice, the adiponectin RNA levels in the eWAT were decreased by 62% and 36% in the $Col18a1^{-/-}$ and $Col18a1^{P2/P2}$ mice, respectively (Fig. 3B). The eWAT adiponectin RNA level was normal in the $Col18a1^{P1/P1}$ mice. Additionally, the *Glut4* RNA levels in the eWAT were markedly reduced in the $Col18a1^{-/-}$ and $Col18a1^{P2/P2}$ mice, by 66% and 57%, respectively, compared with the WT mice. The $Col18a1^{P1/P1}$ mice expressed less *Glut4* RNA in the eWAT than the WT mice, too, but the reduction was smaller than in the other mutant strains (Fig. 3C). *Glut4* is an insulin-regulated glucose transporter found primarily in adipose and striated muscle tissues (Rosen & Xu, 2009). In contrast, transcripts for *Glut2*, the principal glucose transporter in the liver, were increased by 31–40% in the livers of the $Col18a1^{-/-}$ and

Col18a1$^{P2/P2}$ mice (Fig. 3*D*). GLUT2 plays an important role in whole-body glucose homeostasis, and transcription of the hepatic *Glut2* is known to be up-regulated in type 2 diabetes (Im *et al.* 2005). These findings suggest that the adipose tissue dysfunction resulting from the deficiency of medium and long collagen XVIII isoforms may impact whole-body glucose tolerance and insulin sensitivity.

Gluconeogenesis is strongly activated in the liver during fasting and in type 2 diabetes (Rodgers *et al.* 2005). We evaluated several genes primarily expressed in liver and involved in glucose homeostasis and gluconeogenesis. Glucose-6-phosphatase (G6Pase) is a key enzyme responsible for the production of glucose in the liver during fasting or in type 2 diabetes (Im *et al.* 2011). Transcription factor peroxisome proliferator-activated receptor α (PPARα) stimulates hepatic glucose output under energy deprivation and in type 2 diabetes through up-regulation of hepatic G6Pase gene expression (Ferré, 2004; Im *et al.* 2011). Peroxisome proliferator-activated receptor γ coactivator 1 α (PGC1α) regulates hepatic

glucose production through activation of the entire gluconeogenic pathway (Yoon *et al.* 2001; Puigserver *et al.* 2003; Lin *et al.* 2004; Rodgers *et al.* 2005). Kruppel-like factor 15 (KLF15), a transcription factor highly expressed in the liver, regulates the expression of gluconeogenetic genes in coordination with PGC1α (Grey *et al.* 2007; Takashima *et al.* 2010). The above listed genes were all significantly up-regulated in the *Col18a1$^{-/-}$* and/or *Col18a1$^{P2/P2}$* mice livers (Fig. 3*E–H*). These findings indicate that there was increased gluconeogenesis in the mice lacking medium/long collagen XVIII.

The findings observed in the mice lacking either all or the medium and long isoforms of collagen XVIII, namely lipodystrophy, dyslipidaemia, hepatic steatosis and alterations in the expression profiles of key regulators of glucose metabolism, suggest that lack of medium and long variants of collagen XVIII may lead to insulin resistance, impaired glucose tolerance and hyperglycaemia after consuming a HFD. To evaluate glucose intolerance in the mutant mice fed with the HFD, GTTs were
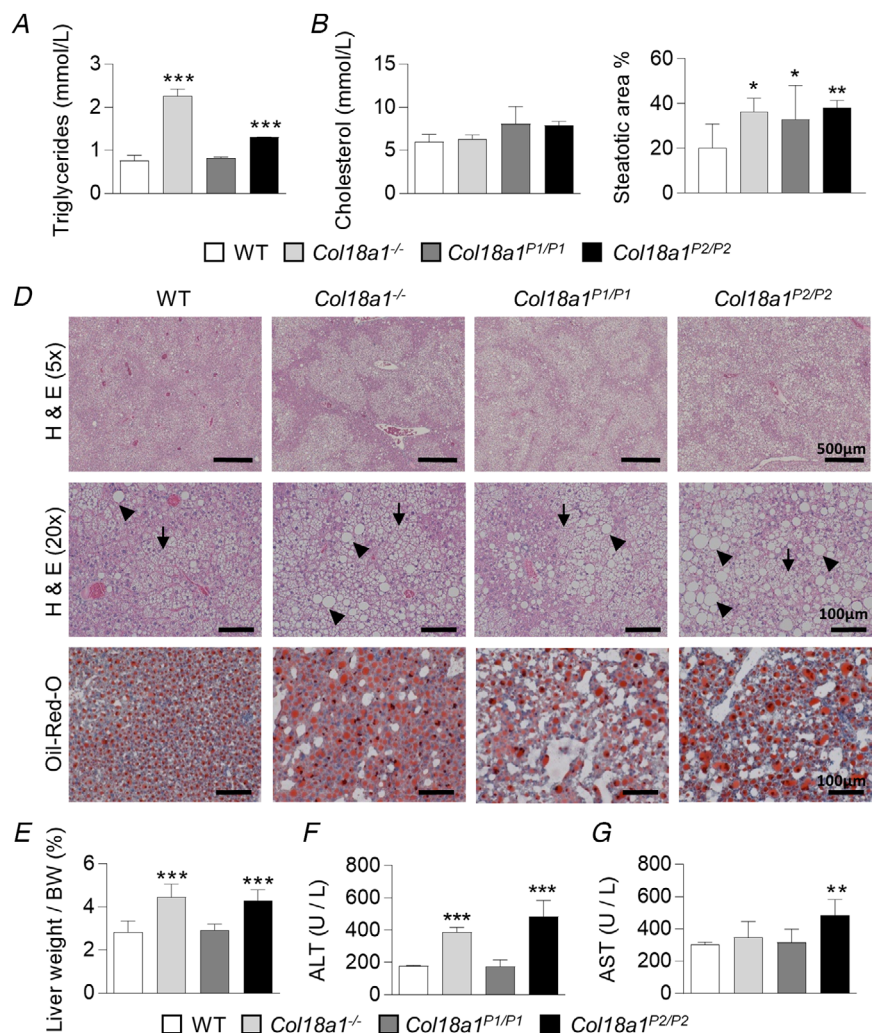

Figure 2. Altered serum lipid profiles, and hepatic steatosis and damage in mice lacking specific collagen XVIII isoforms
Liver and serum analyses of WT, *Col18a1$^{-/-}$*, *Col18a1$^{P1/P1}$* and *Col18a1$^{P2/P2}$* male mice fed on a HFD for 20 weeks. *A* and *B*, serum levels of TGs (*A*) and total cholesterol (*B*); *n* = 4 per genotype. *C*, steatotic area measured from H&E (5×) staining by ImageJ. Two to three images per sample were analysed; *n* = 6–7 per genotype. *D*, representative images of liver sections of the specified genotypes stained with H&E and Oil Red O. Arrows indicate microsteatosis and arrowheads macrosteatosis. Scale bars indicated in the images; *n* = 6–7 per genotype. *E–G*, relative liver weights (*E*), and liver function tests (*F–G*) of the indicated genotypes; ALT (*F*) and AST (*G*) levels in serum; *n* = 6 per genotype. Data are presented as means + SD and statistical significance was tested by one-way ANOVA with Benjamini–Kieger–Yekutieli false discovery rate; *p < 0.05, **p < 0.01, ***p < 0.001. [Colour figure can be viewed at wileyonlinelibrary.com]

performed after fasting the mice for 16 h followed by I.P. injection of 2 g kg^{-1} glucose and consecutive blood glucose measurements at 15, 30, 60 and 120 min after glucose administration (Lamming *et al.* 2012). As anticipated, the glucose levels increased more in the *Col18a1*$^{-/-}$ and *Col18a1*$^{P2/P2}$ mice, indicating impaired glucose tolerance in these mouse strains, whereas the glucose levels of the *Col18a1*$^{P1/P1}$ mice were comparable to those of the WT mice (Fig. 3*I*). The GTTs clearly indicated that the *Col18a1*$^{-/-}$ and *Col18a1*$^{P2/P2}$ mice had an impaired glucose tolerance on the HFD.

Collagen XVIII deficiency impairs glucose tolerance and reduces insulin sensitivity on a standard chow diet

To test the effects of collagen XVIII on glucose metabolism on a standard diet, we assessed fasting glucose and insulin levels, and performed a GTT and a hyperinsulinaemic-euglycaemic clamp. The fasting insulin levels were markedly increased in the *Col18a1*$^{-/-}$ (2.4- and 3.1-fold in males and females, respectively) and *Col18a1*$^{P2/P2}$ mice (3.8- and 5.6-fold in males and females, respectively) fed on a standard diet compared to control mice (Table 2). However, the fasting glucose levels were still normal, suggesting that the increased insulin levels in these mutant mice compensated for the insulin resistance. For each genotype, the basal glucose and insulin levels were similar between male and female mice fed on a standard diet (Table 2), and further experiments were performed using male mice. The GTTs showed that the *Col18a1*$^{-/-}$

and *Col18a1*$^{P2/P2}$ males had significantly impaired glucose tolerance compared with the WT and *Col18a1*$^{P1/P1}$ mice, even on a standard chow (Fig. 4*A*).

The hyperinsulinaemic–euglycaemic clamp (or insulin clamp) is the gold standard method to study insulin resistance (Ayala *et al.* 2011). After an overnight food withdrawal, an insulin clamp procedure was conducted with a primed-continuous infusion of insulin at a constant rate, and glucose was infused at variable rates to maintain plasma glucose at basal concentrations. The exogenous glucose infusion rate to maintain the steady glucose levels was significantly lower in the *Col18a1*$^{-/-}$ and *Col18a1*$^{P2/P2}$ mice than in the WT and *Col18a1*$^{P1/P1}$ mice, indicating different rates of whole-body insulin sensitivity (Fig. 4*B*). This was also confirmed by the markedly slower clearance of [^{14}C]deoxyglucose from blood of the *Col18a1*$^{-/-}$ and *Col18a1*$^{P2/P2}$ mice during the euglycaemic period of the clamp (Fig. 4*C*). Tissue-specific glucose uptake was calculated after the clamp procedure by measuring the amount of [^{14}C]deoxyglucose present in liver, eWAT and soleus muscle. Significantly lower levels of [^{14}C]deoxyglucose were found in the *Col18a1*$^{-/-}$ and *Col18a1*$^{P2/P2}$ livers (Fig. 4*D*). Also, eWAT showed impaired, albeit statistically insignificant, glucose uptake in *Col18a1*$^{-/-}$ and *Col18a1*$^{P2/P2}$ mouse strains, consistent with low expression of *Glut4* in this tissue, while in the skeletal muscles of these mice, glucose uptake was increased. Taken together, the glucose and insulin measurements indicate that the lack of specific collagen XVIII variants leads to abnormal glucose metabolism, manifested as glucose intolerance and impaired insulin
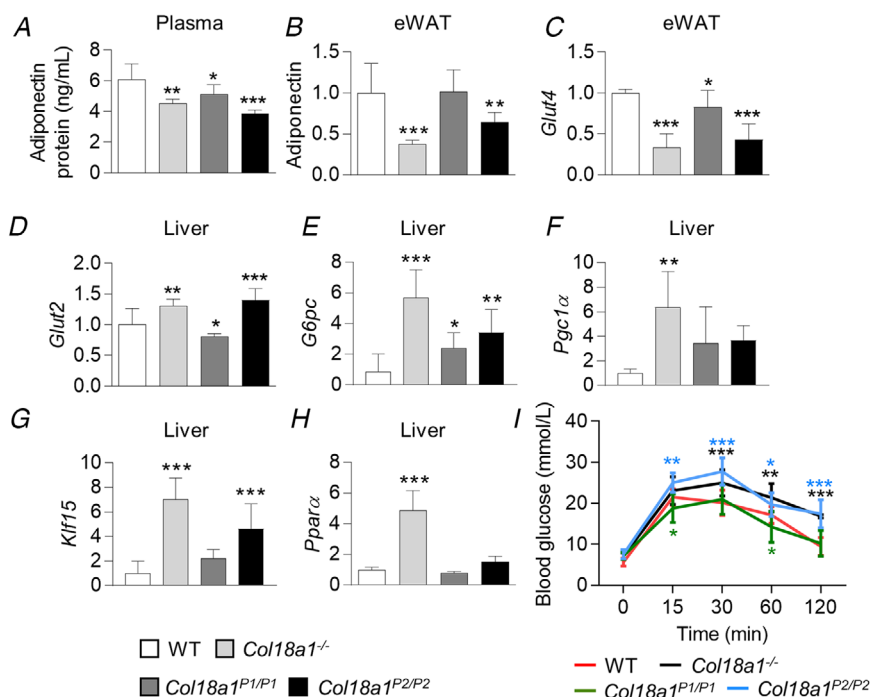

Figure 3. Lack of collagen XVIII induces changes in glucose and lipid homeostasis
Protein and gene expression analysis of WT and mutant mice on a HFD for 20 weeks. (*A*) Plasma protein levels of adiponectin. *B* and *C*, relative RNA expression levels of adiponectin (*B*) and *Glut4* (*C*) in eWAT. *D–H*, relative RNA levels of *Glut2* (*D*), *G6pc* (*E*), *Pgc1α* (*F*), *Klf15* (*G*) and *Pparα* (*H*) in liver. Gene expression levels were analysed by RT-qPCR. Data were normalized to β-actin or 18S ribosomal RNA and compared against WT mice. In *A–G*, $n = 5$–8 per genotype. Data presented as means + SD. *I*, intraperitoneal glucose tolerance tests of WT and mutant mice on a HFD. WT, $n = 11$; *Col18a1*$^{-/-}$, $n = 6$; *Col18a1*$^{P1/P1}$, $n = 6$; *Col18a1*$^{P2/P2}$, $n = 8$. Data are presented as mean + SD. Statistical significance was tested with one-way or two-way ANOVA with Benjamini–Kieger–Yekutieli false discovery rate; *$p < 0.05$; **$p < 0.01$; ***$p < 0.001$. eWAT, epididymal white adipose tissue. [Colour figure can be viewed at wileyonlinelibrary.com]

Table 2. Basal blood glucose and plasma insulin values in 20-week-old WT and collagen XVIII mutant mice fed on standard chow

Genotype	Glucose (mmol l^{-1})		Insulin (ng ml^{-1})	
	Male	Female	Male	Female
WT	5.30 ± 0.17	4.65 ± 0.84	1.35 ± 1.01	0.94 ± 0.68
Col18a1$^{-/-}$	4.65 ± 0.66	4.00 ± 0.59	3.29 ± 0.61[**]	2.88 ± 0.43[*]
Col18a1$^{P1/P1}$	5.88 ± 0.46	5.38 ± 0.21	1.82 ± 0.39	1.28 ± 0.45
Col18a1$^{P2/P2}$	5.26 ± 0.84	5.05 ± 0.97	5.10 ± 2.13[**]	5.28 ± 0.54[*]

Blood was drawn from the saphenous vein after 16 h of fasting and assessed for the parameters above. Values are means ± SD, $n = 5$–10. [*]$P < 0.05$; [**]$P < 0.01$; WT *vs. Col18a1*$^{-/-}$; WT *vs. Col18a1*$^{P2/P2}$ mice compared with same sex.

sensitivity, in addition to the previously observed defect in adipocyte differentiation (Fukai *et al.* 2002; Aikio *et al.* 2014).

Collagen XVIII-deficient mice show increased non-shivering thermogenesis

As described above, the *Col18a1*$^{-/-}$ mice consumed the same amount of food in the HFD, but their body weight gain was slower than that in the WT mice, even if the mutants showed similar physical activity to the controls (Fig. 1). Based on these findings, we considered the possibility that the *Col18a1*$^{-/-}$ mice had increased their energy consumption by non-shivering thermogenesis in the BAT. Cold is an efficient activator of BAT, and therefore we exposed the WT and *Col18a1*$^{-/-}$ mutant mouse lines to cold (+4°C) in metabolic cages for 7 days, and monitored gas exchange, activity and food consumption during the cold exposure. These studies showed that *Col18a1*$^{-/-}$ mice generated more heat than the WT mice over the course of the experiment (Fig. 5*A*)
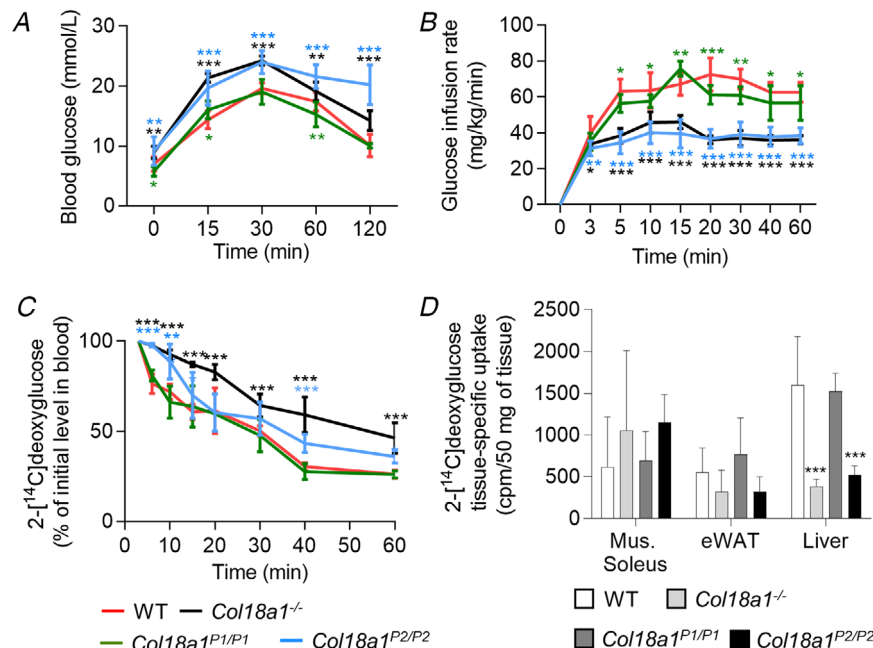

Figure 4. Collagen XVIII deficiency alters glucose metabolism on a standard chow diet
A, glucose tolerance test on WT and *Col18a1* mutant mice fed with a standard chow diet; $n = 10$ per genotype, and data are presented as means + SD. *B–D*, hyperinsulinaemic–euglycaemic clamp studies. *B*, glucose infusion rates necessary to maintain euglycaemia during the insulin clamp procedure with 26-week-old mice. *C*, insulin-stimulated whole-body glucose uptake. The amount remaining of 2-[^{14}C]deoxyglucose in blood at indicated time points after an initial glucose bolus compared with the initial level. In *B* and *C*, $n = 6$ per genotype. Data are presented as means ± SD. *D*, glucose uptake by soleus muscle, eWAT and liver. Results are presented as counts per minute (cpm)/50 mg of tissue; $n = 6$ per genotype, and data are presented as means + SD. Statistical significance was tested with one-way or two-way ANOVA with Benjamini–Kieger–Yekutieli false discovery rate; [*]$p < 0.05$; [**]$p < 0.01$; [***]$p < 0.001$. eWAT, epididymal white adipose tissue. [Colour figure can be viewed at wileyonlinelibrary.com]

and the physical activity of the *Col18a1*$^{-/-}$ mice was also higher than their controls (Fig. 5*B*). However, it should be noted that the *Col18a1*$^{-/-}$ mice had higher heat production than the WT mice during the 7 days' cold adaptation at +18°C, while their physical activities were equal during this period (data not shown). Interestingly, the respiratory exchange rate (RER) showed differences between the WT and *Col18a1*$^{-/-}$ mice; it decreased in the WT mice and increased in the *Col18a1*$^{-/-}$ mice during the cold exposure (Fig. 5*C*). This finding suggests that WT mice increase the use of lipids in cold, while *Col18a1*$^{-/-}$ mice begin to favour carbohydrates as the energy source in these conditions. Food consumption (Fig. 5*D*) and body weights (Fig. 5*E*) showed no differences amongst the genotypes, excluding the possible effects of these factors on the altered RER profile in the *Col18a1*$^{-/-}$ mice compared with controls. Analysis of the tissues collected

after the cold exposure showed that the *Col18a1*$^{-/-}$ mice had a significantly increased interscapular BAT weight (Fig. 5*F*), suggestive of increased activation of the BAT, while iWAT and eWAT weights showed no statistically significant differences among the genotypes. Interestingly, the observed high serum TG levels of the *Col18a1*$^{-/-}$ mice, both on a normal chow (Aikio *et al.* 2014) and on a HFD (Fig. 2*A*), decreased to the level of the WT mice during the cold exposure, suggesting an improved TG clearance in the KO mice due to the increased heat production (Fig. 5*G*). The serum free fatty acid (FFA) concentrations were similar between the genotypes, indicative of similar lipolytic activity in both mouse lines (Fig. 5*H*).

As many of the metabolic defects observed in the *Col18a1*$^{-/-}$ mice, i.e. high TGs, liver damage and insulin resistance (Figs 2 and 4) and impaired adipocyte differentiation (Aikio *et al.* 2014), were also observed in
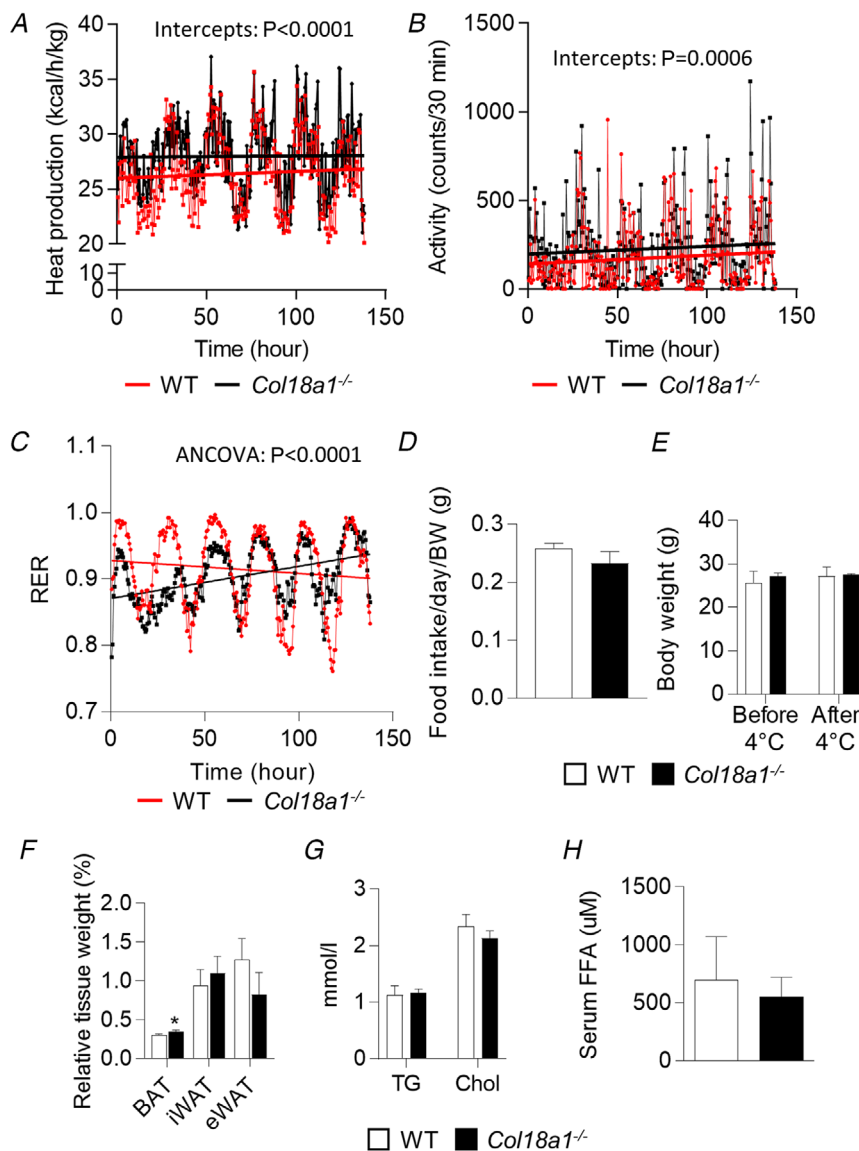

Figure 5. Metabolic analysis of *Col18a1*$^{-/-}$ and WT mice during cold exposure

A–D, 14- to 15-week-old male mice were subjected to cold at +4°C for 7 days, and heat production (normalized to the body weight) (*A*), physical activity (*B*), RER (*C*) and food intake (*D*) were measured. *E*, body weights before and after the cold exposure. *F–H*, relative adipose tissue weights (% of adipose tissue of the body weight) (*F*), serum TG and cholesterol levels (*G*) and FFA concentrations (*H*) after the cold exposure. In *A–H*, n = 3 per genotype. *A–C*, data are presented as means only and statistical significance tested with ANCOVA. *D–H*, data are presented as means + SD and statistical significance was tested with Student's unpaired *t* test; *$p < 0.05$. BAT, brown adipose tissue; Chol, cholesterol; eWAT, epididymal white adipose tissue; FFA, free fatty acid; iWAT, inguinal white adipose tissue; TG, triglycerides. [Colour figure can be viewed at wileyonlinelibrary.com]

the $Col18a1^{P2/P2}$ mice, we subjected the $Col18a1^{P2/P2}$ mice to cold exposure. The heat production and the physical activity were higher in the $Col18a1^{P2/P2}$ mice compared with the WT mice (Fig. 6A and B), and similarly to the $Col18a1^{-/-}$ mice, the RER values of the $Col18a1^{P2/P2}$ mice increased during the cold exposure (Fig. 6C). The food intake was similar between the genotypes (Fig. 6D). The body weight of the $Col18a1^{P2/P2}$ mice was slightly lower than that of the WT mice in the beginning of the experiment but showed no difference after the cold exposure (Fig. 6E). The relative adipose tissue weights (Fig. 6F) did not show significant differences between the $Col18a1^{P2/P2}$ and the control mice. However, the eWAT weights of the $Col18a1^{P2/P2}$ tended to slightly decrease, and their BAT and iWAT weights increased, thus resembling the values of the corresponding $Col18a1^{-/-}$ tissues and being in line with our previously reported findings (Aikio

et al. 2014). Unlike in the $Col18a1^{-/-}$ mice, the high TG levels of the $Col18a1^{P2/P2}$ mice (Aikio et al. 2014; Fig. 2A) did not revert to a normal level during cold exposure but remained about 60% higher than TG levels in the WT mice (Fig. 6G). The cholesterol levels and the FFA concentrations showed no changes among the genotypes (Fig. 6G and H). These findings indicate that the lack of collagen XVIII and especially its P2 derived isoforms leads to the increased heat production in the cold and reduction of the abnormally high blood TG levels in the case of total collagen XVIII deficiency.

Brown and beige adipose tissues show subtle activation in the absence of collagen XVIII

Cold enhances the TG clearance from the blood by increasing fatty acid uptake, particularly into BAT (Bartelt
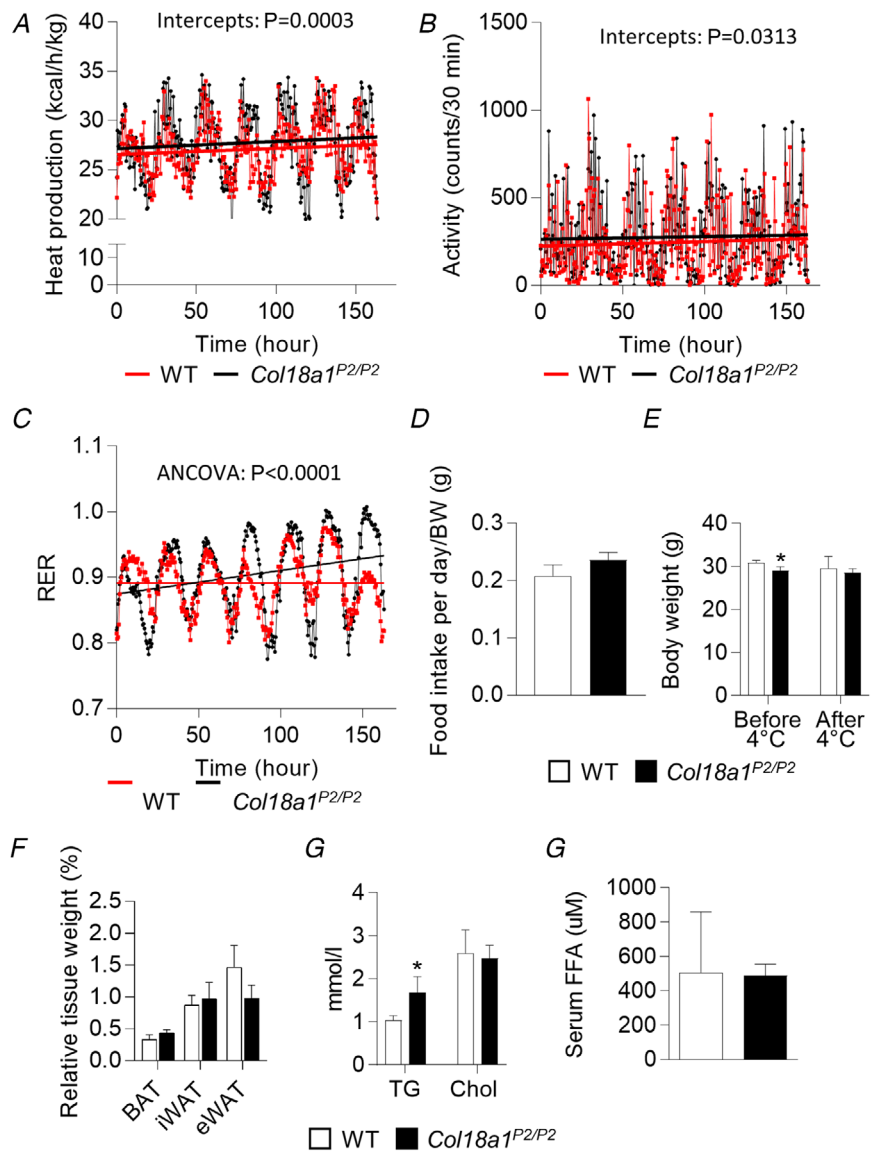

Figure 6. Metabolic analysis of the $Col18a1^{P2/P2}$ KO mice during the cold exposure
The 14- to 15-week-old male mice were subjected to cold at $+4°C$ and metabolic and behavioural parameters were recorded for 7 days. A–D, heat production (normalized to the body weight) (A), physical activity (B), RER (C) and food intake (D) were measured in the metabolic cages. E, body weights are presented before and after the cold exposure. F–H, weights of the adipose tissues (% of adipose tissue of the body weight) (F), serum TG and cholesterol levels (G) and FFA concentrations (H) were measured after the cold exposure. In A–H, $n = 4$ per genotype. A–C, data are presented as means only and statistical significance tested with ANCOVA. D–G, data are presented as means $+$ SD and statistical significance was tested with Student's unpaired t test. $*p < 0.05$. BAT, brown adipose tissue; Chol, cholesterol; eWAT, epididymal white adipose tissue; FFA, free fatty acids; iWAT, inguinal white adipose tissue; TG, triglycerides. [Colour figure can be viewed at wileyonlinelibrary.com]

et al. 2011). Thus, we studied the thermogenic adipose tissues to investigate their role in TG clearance, altered RER values and increased heat production, which were observed in the *Col18a1*$^{-/-}$ and *Col18a1*$^{P2/P2}$ mice. As mentioned above, the BAT size was significantly increased in the *Col18a1*$^{-/-}$ mice upon cold exposure. However, histological analysis revealed no major morphological changes in the BAT amongst the genotypes (Fig. 7*A*), and immunostaining against UCP1 showed an even localization of UCP1 in all BAT samples, though the staining appeared most intense in the *Col18a1*$^{P2/P2}$ samples (Fig. 7*A*). To further assess potential BAT activation in the different genotypes, we measured transcript levels of several thermogenesis- and brown fat phenotype-related genes (*Ucp1, Cidea, Dio2, Pgc-1a* and *Cox7a1*) to evaluate BAT activity (Seale *et al.* 2007). These results showed a trend for increased *Ucp1* and *Cidea* expression in the *Col18a1*$^{-/-}$ and *Col18a1*$^{P2/P2}$ mice, indicative for a higher BAT activity in these strains (Fig. 7*B* and *C*).

Subcutaneous iWAT is also sensitive to cold and prone to undergo modifications towards beige adipose tissue (Nedergaard *et al.* 2019), which can contribute to the heat production and blood TG clearance. H&E staining showed no differences amongst the genotypes in the iWAT samples after cold exposure. However, browning of all iWATs was evident and confirmed by immunohistochemical detection of UCP1. This staining showed a local abundance of UCP1 in the iWAT samples (Fig. 7*D*), whereas the eWAT samples showed no detectable UCP1 signals and no differences in the histology in the WT and *Col18a1*$^{-/-}$ samples (data not shown). Similar to the BAT, a trend (though not reaching statistical significance) for up-regulation of expression of genes related to thermogenesis and adipose tissue browning was observed in the iWAT of the *Col18a1*$^{-/-}$ and the *Col18a1*$^{P2/P2}$ mice compared to the WT samples; for example *Ucp1* and *Cidea* showed up to fourfold increases in the *Col18a1*$^{-/-}$ mice and were increased also in the *Col18a1*$^{P2/P2}$ mice (Fig. 7*E* and *F*). Taken together, the observed increase in the BAT mass in the *Col18a1*$^{-/-}$ mice and the slightly increased activation of BAT/iWAT in the *Col18a1*$^{-/-}$ and *Col18a1*$^{P2/P2}$ mice may explain the increased heat production, TG clearance and altered RER values in these mouse strains.

In addition to these classic thermogenic tissues, muscle has been shown to contribute to the non-shivering heat production. Sarcolipin is a small peptide found in the sarcoplasmic reticulum and it has been shown to direct muscle non-shivering thermogenesis by regulating sarco/endoplasmic reticulum Ca^{2+}-ATPase (SERCA) activity (Bal *et al.* 2012; Chouchani *et al.* 2019). We measured the expression of these genes in the muscle and found no differences between the genotypes (Fig. 8*A* and *B*). These results indicate that muscles do not contribute to the increased heat production detected in
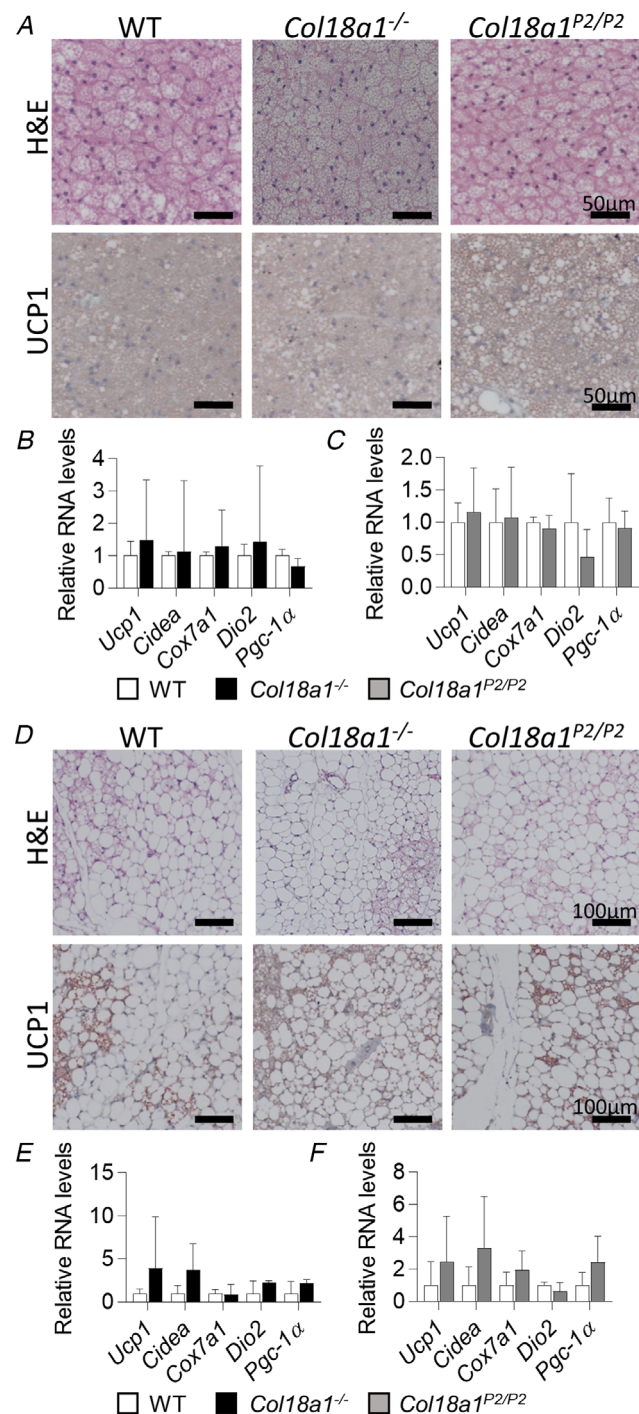

Figure 7. Analyses of BAT and iWAT after the cold exposure
A and *D*, representative images of H&E and UCP1 staining of BAT (*A*) and iWAT after the cold exposure at 4 °C for 7 days (*D*). Scale bars 50 μm (*A*) or 100 μm (*D*). *B, C, D* and *F*, RT-qPCR analysis of the indicated genes related to the thermogenic capacity and BAT activity in BAT (*B* and *C*) and in iWAT (*E* and *F*). RNA levels were normalized to the *PPIA* expression and shown relative to the WT samples. *n* = 3–4 per genotype. Data are presented as means + SD and statistical significance was tested with Student's unpaired *t* test. BAT, brown adipose tissue; iWAT, inguinal white adipose tissue; PPIA, peptidylprolyl isomerase A. [Colour figure can be viewed at wileyonlinelibrary.com]

the in *Col18a1*$^{-/-}$ and *Col18a1*$^{P2/P2}$ mice during the cold exposure.

Lipolysis is not affected in collagen XVIII-deficient mice

We have shown that the collagen XVIII deficiency impairs the adipogenetic capacity of the mice (Aikio *et al.* 2014) but whether the lipolytic response in adipose tissue is affected remains to be resolved. A β-adrenergic agonist, NA, stimulates lipolysis by releasing FFA and glycerol from TGs, and activates BAT, thereby mimicking an acute cold exposure (Chouchani *et al.* 2019). We detected no differences in serum FFA concentrations between the *Col18a1*$^{-/-}$ mice and the WT mice, before or after 35 min of NA stimulation (Fig. 9*A*). Rectal body temperature, measured during the NA stimulation, showed no differences between the genotypes either (Fig. 9*B*). In addition, the lipolytic capacity of the WT and *Col18a1*$^{-/-}$ primary adipocytes was measured *in vitro*. The amount of glycerol released from adipocytes into the cell culture medium upon NA treatment was found to be similar between the genotypes (Fig. 9*C*). Altogether, the mice lacking collagen XVIII have similar responses to the β-adrenergic stimulation to WT mice, suggesting that collagen XVIII deficiency does not affect lipolytic capacity.
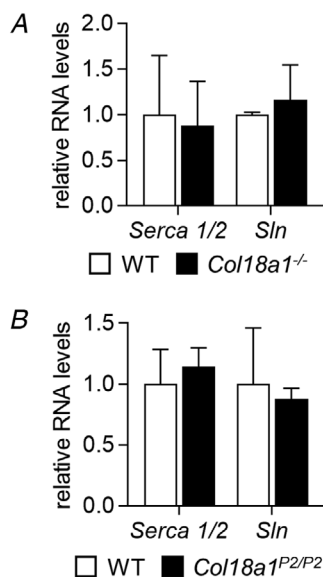

Figure 8. qPCR analysis of muscle tissues after cold exposure
RNA expression levels of genes related to non-shivering thermogenesis in skeletal muscles after chronic cold exposure. The RNA levels of *Serca 1* and *2* (*Serca 1/2*) and *sarcolipin* (*Sln*) were normalized to the *PPIA* expression and shown relative to the WT samples. *n* = 3–4 per genotype. Data are presented as means + SD and statistical significance was tested with Student's unpaired *t* test. PPIA, peptidylprolyl isomerase A.

Collagen XVIII-deficient mice show ultrastructural changes in BAT

Ultrastructural studies by transmission electron microscopy revealed changes in the BAT composition in the collagen XVIII-deficient mice. Specifically, the *Col18a1*$^{-/-}$ and *Col18a1*$^{P2/P2}$ mice had a higher cytoplasmic content in the BAT at room temperature (Fig. 10*A* and *B*). To investigate the effect of cold, we analysed the ultrastructure of BAT samples after the cold exposure. Representative images of each genotype are shown in the Fig. 10*C*. Quantification of the cytoplasmic area revealed similar results to those we obtained from the mice at room temperature; the *Col18a1*$^{-/-}$ mice exhibited a trend for an increased cytoplasmic area when compared with WT mice (Fig. 10*D*). Interestingly, the percentages of the cytoplasmic content did not change in the BAT of the *Col18a1*$^{-/-}$ mice during the cold exposure. The WT mice had about 30% cytoplasm at both temperatures, and the *Col18a1*$^{-/-}$ mice had about 40% cytoplasm. The *Col18a1*$^{P2/P2}$ mice showed no difference in the cytoplasmic content compared with the WT mice at room temperature (Fig. 10*D*). To assess whether the increased cytoplasmic area reflected a higher mitochondrial content in the collagen XVIII-deficient BAT, we estimated the mitochondrial to nuclear DNA ratio by measuring the expression of the mitochondrial gene *Nd1* by RT-qPCR and normalized the gene expression to the nuclear gene *PPIA*. The *Col18a1*$^{-/-}$ and *Col18a1*$^{P2/P2}$ mice had a tendency towards an increased mtDNA compared with the WT mice in BAT (Fig. 10*E*). Comparable results were also obtained from the iWAT samples collected after cold exposure; the *Col18a1*$^{-/-}$ and *Col18a1*$^{P2/P2}$ mice showed a trend for increased mitochondrial content (Fig. 10*F*). Taken together, our findings on the increased amount of BAT in collagen XVIII-deficient mice and its higher mitochondrial content could explain the increased heat generation and clearance of serum TG of collagen XVIII-deficient mice in the cold temperature.

Discussion

In this study, we assessed the metabolic consequences of the reduced adiposity associated with collagen XVIII-deficient mice. Our data indicated that feeding the *Col18a1*$^{-/-}$ mice with a long-term high calorie diet led to significant lipodystrophy and, consequently, to a pre-diabetic condition with insulin resistance and impaired glucose tolerance in the mutant mice. Due to the limited capacity of the *Col18a1*$^{-/-}$ mice to store the excess dietary fat in adipocytes, the TGs remained in circulation and accumulated in the liver, causing dyslipidaemia and hepatosteatosis. Interestingly, at the cold temperature, *Col18a1*$^{-/-}$ mice showed increased heat

production compared with the control WT mice, and their high blood TG levels reverted to the level of the WT mice.

In addition to the $Col18a1^{-/-}$ mice, the $Col18a1^{P2/P2}$ mice, lacking specifically the medium and long isoforms, exhibited resistance to a long-term HFD-induced fat mass accrual (Fig. 1A and B), an observation in line with the previously found defect in adipocyte differentiation in this mouse line (Aikio *et al.* 2014). The current investigations further confirmed that the lack of P2-driven expression of medium and long collagen XVIII, the main isoforms produced in the liver and eWAT, results in ectopic fat accumulation in the liver and high plasma TG levels on a long-term HFD, whereas the short collagen XVIII appears to have minor, if any, role in lipid metabolism (Fig. 2).

Coinciding with the reduced adiposity, circulating protein levels and RNA levels of the adipose tissue-specific adiponectin hormone were greatly reduced in $Col18a1^{-/-}$ mice, as well as in $Col18a1^{P2/P2}$ mice. Adiponectin is necessary for proper insulin sensitivity, and its deficiency is associated with the development of type 2 diabetes (Chao *et al.* 2000; Berg *et al.* 2002; Gavrilova *et al.* 2003). Thus, our findings on low insulin sensitivity in the $Col18a1^{-/-}$ and $Col18a1^{P2/P2}$ mice (Figs 3I and 4) coincides with the low adiponectin levels. Poor insulin sensitivity results in increased insulin secretion by the pancreas to compensate for insulin resistance (Kahn, 2003; Tripathy *et al.* 2004), and this was observed in the $Col18a1^{-/-}$ and $Col18a1^{P2/P2}$ mice, which showed a severalfold increase in circulating plasma insulin levels on a standard chow diet (Table 2).

In addition, our data indicated an increase in hepatic gluconeogenesis in the $Col18a1^{-/-}$ and $Col18a1^{P2/P2}$ mice fed with a HFD demonstrated by up-regulation of several genes involved in the regulation of gluconeogenesis (Fig. 3). Up-regulated gluconeogenesis characterizes hepatic insulin resistance, which can be caused by the increased lipid content in the liver (Perry *et al.* 2014). Given that enhanced gluconeogenesis causes increased glycaemia, it was not surprising that the expression of *Glut2* was elevated in the $Col18a1^{-/-}$ and $Col18a1^{P2/P2}$ mouse livers. On the other hand, the expression of the insulin-regulated glucose transporter *Glut4* was decreased in the adipose tissues of the $Col18a1^{-/-}$ and the $Col18a1^{P2/P2}$ mice on HFD, impeding the transport of glucose to adipocytes for lipogenesis. These findings are similar to those for insulin-resistance states, including obesity and type 2 diabetes (Shepherd & Kahn, 1999; Abel *et al.* 2001; Minokoshi *et al.* 2003). In addition, glucose concentrations remained significantly higher in the $Col18a1^{-/-}$ and $Col18a1^{P2/P2}$ mice when the GTT was performed on the HFD or standard chow (Figs 3J and 4). It is known that tissues differ in their responses to insulin. In muscle, insulin resistance typically leads to reduced glucose uptake and muscle glycogen formation, while in WAT, it lowers the insulin-mediated suppression of lipolysis in addition to decreasing the glucose uptake (Mu *et al.* 2019). Our euglycaemic clamp
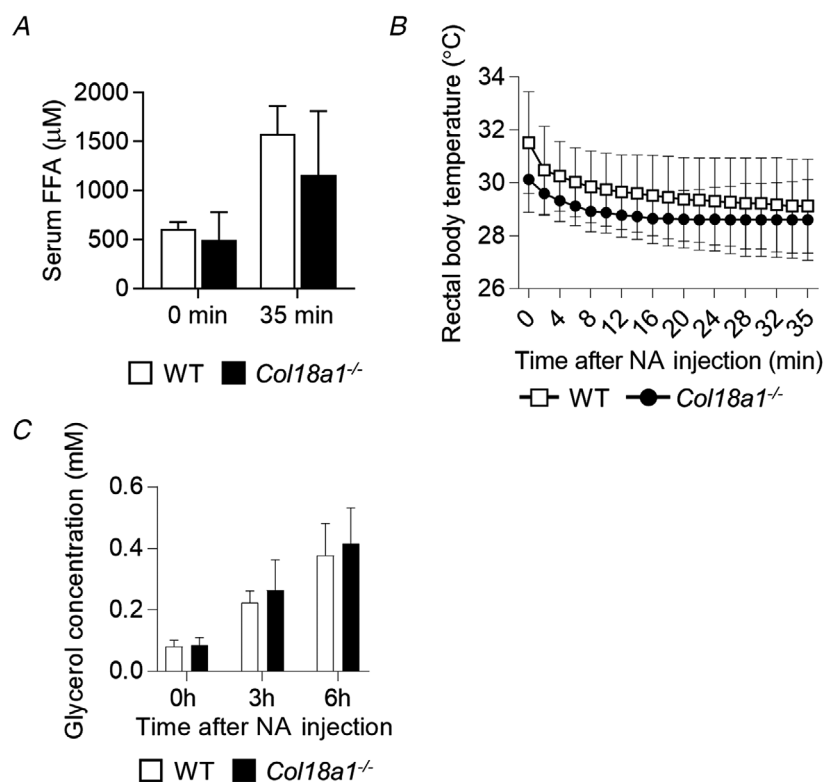

Figure 9. Lipolytic capacity is not affected in collagen XVIII knockout mice
The response to noradrenaline (NA) stimulation was studied with 12-week-old male mice fasted 24 h before the NA treatment. *A*, serum FFA concentrations were measured before and after 35 min of NA injection. *B*, rectal body temperatures were recorded during the stimulation. *C*, glycerol content in the cell culture medium of differentiated preadipocytes was measured after NA treatment. $n = 3–4$ per genotype/cell line. Data are presented as means + SD and statistical significance was tested with Student's unpaired *t* test (*A* and *C*) or two-way ANOVA (*B*). FFA, free fatty acids.

study suggested that the skeletal muscles of the mice lacking the medium and long collagen XVIII are sensitive to insulin (Fig. 4*D*), but further studies are needed to demonstrate the roles of collagen XVIII in muscles and the pancreas. Altogether, our current findings indicate that, in the *Col18a1*$^{-/-}$ and *Col18a1*$^{P2/P2}$ mice, changes in the adipose tissue and liver can largely explain the observed insulin resistance and glucose intolerance. Nevertheless, it is important to clarify the impact of collagen XVIII in hepatic insulin resistance at the molecular level by studying its effects of major insulin signalling pathways, including the phosphoinositide-3-kinase–protein kinase B/Akt pathway (Perry *et al.* 2014).

Free fatty acids circulating in the blood can cause insulin resistance, and patients with type 2 diabetes need lower doses of anti-diabetic drugs if their high blood TG levels are normalized (Dresner *et al.* 1999; Rachek, 2014; Parhofer, 2015). Cold exposure is an efficient means to clear the blood lipids by increasing BAT activity (Bartelt *et al.* 2011). We observed a higher BAT mass in the *Col18a1*$^{-/-}$ mice than in the WT mice after cold exposure (Fig. 5*F*), suggesting enhanced thermogenesis in the absence of collagen XVIII (Kalinovich *et al.* 2017). Indeed, heat production was more effective in the *Col18a1*$^{-/-}$ and the *Col18a1*$^{P2/P2}$ mice than in the WT mice in the cold (Figs 5*A* and 6*A*). The increased cytoplasmic area and mitochondrial content suggested more active BAT in these

mutant mice at room temperature (Fig. 10). After the cold exposure the trend for an increased cytoplasmic area was detected only in the total *Col18* knock-out mice even though the slightly increased expression levels of the *Ucp1* gene were detected in both *Col18a1*$^{-/-}$ and the *Col18a1*$^{P2/P2}$ mice (Fig. 7*B* and *C*). UCP1 is activated by long-chain fatty acids that are produced within brown adipocytes through lipolysis (Cannon & Nedergaard, 2004). However, recently Shin *et al.* (2017) showed that the intracellular lipolysis in brown or white adipocytes is not necessary for the non-shivering thermogenesis in BAT, but TGs can be taken up from blood and used in heat production. Thus, the increased thermogenesis detected in the *Col18a1*$^{-/-}$ mice might be a secondary effect of the high blood TG levels, via enhanced substrate availability to UCP1, and it thereby activated non-shivering thermogenesis.

In the cold exposure, the *Col18a1*$^{-/-}$ mice apparently consumed the excess of circulating lipids first and then began to favour carbohydrates as an energy source as the cold exposure progressed. This change was seen in the increasing RER value during the cold exposure (Fig. 5*C*). In contrast, the decreasing RER value of the WT mice indicated that they increased the lipolysis during the cold exposure to compensate for the increased fatty acid uptake from the blood (Shin *et al.* 2017). As expected, the RER of the *Col18a1*$^{P2/P2}$ mice behaved similarly to that
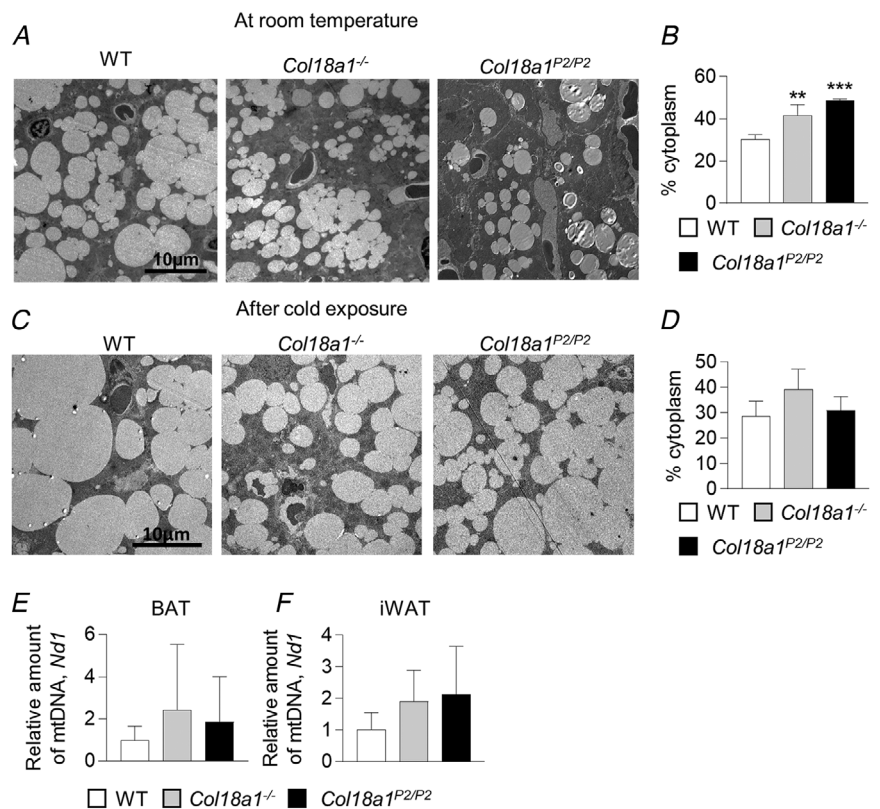

Figure 10. Collagen XVIII deficiency increases the cytoplasmic area in BAT
A–D, representative transmission electron microscopy images of BAT and relative amount of cytoplasm in BAT at room temperature (*A* and *B*) and after cold exposure (*C* and *D*). *E* and *F*, relative amount of mtDNA was measured by RT-qPCR in BAT (*E*) and iWAT (*F*) samples after the cold exposure. Expression levels were normalized to *PPIA* and are shown relative to WT samples. In *A–F*, *n* = 3–4 per genotype. Data are presented as mean + SD and statistical significance was tested with one-way ANOVA (*B*, *D–F*). BAT, brown adipose tissue; iWAT, inguinal white adipose tissue; PPIA, peptidylprolyl isomerase A.

of the $Col18a1^{-/-}$ mice, thus matching the finding that both genotypes have high blood TGs (Figs 6 and 2*A*). However, lipolytic capacity and the ability to respond to β-adrenergic stimulation were not affected in the collagen XVIII-deficient mice or primary adipocytes derived from them (Fig. 9). Higher energy expenditure via thermogenesis could explain the lower body weight gain of the $Col18a1^{-/-}$ mice, although they ate the same amount of food compared with WT controls that we saw in the HFD. Studies with mice have shown that increased BAT activity improves the metabolic profile and decreases fat mass (Liu *et al.* 2015). Consistently in humans, repeated cold exposure elevates energy expenditure by increasing non-shivering thermogenesis (van der Lans *et al.* 2013), and the activity of BAT negatively correlates with fat mass (Cypess *et al.* 2009; Brendle *et al.* 2018). Additionally, active BAT takes up fatty acids and efficiently lowers TG levels in blood (Bartelt *et al.* 2011), which also supports our findings.

The ECM is a key regulator of adipogenesis, and adipocytes extensively remodel their environment (Mariman & Wang, 2010). Increased ECM protein expression in adipose tissue and liver is associated with the development of insulin resistance and with the development of type 2 diabetes. For example, the amount of collagen I and III increases in adipose tissue and liver in obese mice (Williams *et al.* 2015). Moreover, fibrillar collagen V, specifically its less abundant $\alpha1(V)\alpha2(V)\alpha3(V)$ heterotrimer, associates with metabolic dysfunctions. Thus, ablation of the *Col5a3* gene causes similar defects as we observed in the $Col18a1^{-/-}$ mice, including reduced adipose tissue mass, resistance to HFD-induced weight gain, impaired glucose tolerance and reduced insulin sensitivity. *Col5a3* KO mice have a reduced β-cell area in the pancreas resulting in the decreased insulin production and secretion. Moreover, insulin-induced glucose uptake is diminished in the adipose tissue and skeletal muscle, and insulin signalling is reduced in these tissues and in pancreas as well (Huang *et al.* 2011). These results partly differ from our observations in the $Col18a1^{-/-}$ and the $Col18a1^{P2/P2}$ mice which secrete more insulin, possibly to compensate the decreased insulin sensitivity in WAT and liver. In addition to collagens, lack of some other ECM proteins, for example, thrombospondin and osteopontin, sensitizes the insulin signalling and prevents HFD-induced obesity in mice (Williams *et al.* 2015). Compared with these examples, collagen XVIII has more complex effects on metabolism, as its lack impairs insulin sensitivity, but protects the mice from HFD-induced obesity. We suggest that the lack of collagen XVIII primarily causes defects in adipose tissue development (Aikio *et al.* 2014) and that the observed lipodystrophy causes secondary effects, i.e. fatty liver and impaired insulin sensitivity as also detected in other lipodystrophic mice models (Cortes *et al.* 2009; Wang *et al.* 2013). Future studies with conditional *Col18a1*

KO mice, once available, will allow a specific deletion of collagen XVIII in liver or in WAT, and conclusive support for this suggestion.

In summary, our study demonstrated that the absence of collagen XVIII, and largely lack of the P2-derived isoforms, leads to typical signs of metabolic syndrome, namely insulin resistance, glucose intolerance and elevated serum TG levels, likely through markedly reduced adiposity accompanied by accumulation of lipids in hepatocytes. This differs mechanistically from obesity-induced metabolic syndrome. In cold, collagen XVIII-deficient mice utilized the abundant serum TGs as the energy source for non-shivering thermogenesis in the BAT. More generally, these findings highlight the role of ECM proteins as regulators of glucose and lipid metabolism, and specifically warrant analyses of collagen XVIII expression and potential mutations in humans with metabolic syndrome, diabetes, atherosclerosis, lipodystrophies and hepatic disorders.

References

Abel ED, Peroni O, Kim JK, Kim YB, Boss O, Hadro E, Minnemann T, Shulman GI & Kahn BB (2001). Adipose-selective targeting of the GLUT4 gene impairs insulin action in muscle and liver. *Nature* **409**, 729–733.

Aikio M, Elamaa H, Vicente D, Izzi V, Kaur I, Seppinen L, Speedy HE, Kaminska D, Kuusisto S, Sormunen R, Heljasvaara R, Jones EL, Muilu M, Jauhiainen M, Pihlajamaki J, Savolainen MJ, Shoulders CC & Pihlajaniemi T (2014). Specific collagen XVIII isoforms promote adipose tissue accrual via mechanisms determining adipocyte number and affect fat deposition. *Proc Natl Acad Sci U S A* **111**, E3043–E3052.

Akinci B, Meral R & Oral EA (2018). Phenotypic and genetic characteristics of lipodystrophy: pathophysiology, metabolic abnormalities, and comorbidities. *Curr Diab Rep* **18**, 143–149.

Asterholm IW, Halberg N & Scherer PE (2007). Mouse models of lipodystrophy key reagents for the understanding of the metabolic syndrome. *Drug Discov Today Dis Models* **4**, 17–24.

Ayala JE, Bracy DP, Malabanan C, James FD, Ansari T, Fueger PT, McGuinness OP & Wasserman DH (2011). Hyperinsulinemic-euglycemic clamps in conscious, unrestrained mice. *J Vis Exp* (57), 3188.

Bal NC, Maurya SK, Sopariwala DH, Sahoo SK, Gupta SC, Shaikh SA, Pant M, Rowland LA, Bombardier E, Goonasekera SA, Tupling AR, Molkentin JD & Periasamy M (2012). Sarcolipin is a newly identified regulator of muscle-based thermogenesis in mammals. *Nat Med* **18**, 1575–1579.

Bartelt A, Bruns OT, Reimer R, Hohenberg H, Ittrich H, Peldschus K, Kaul MG, Tromsdorf UI, Weller H, Waurisch C, Eychmuller A, Gordts PL, Rinninger F, Bruegelmann K, Freund B, Nielsen P, Merkel M & Heeren J (2011). Brown adipose tissue activity controls triglyceride clearance. *Nat Med* **17**, 200–205.

Berg AH, Combs TP & Scherer PE (2002). ACRP30/adiponectin: an adipokine regulating glucose and lipid metabolism. *Trends Endocrinol Metab* **13**, 84–89.

Bishop JR, Passos-Bueno MR, Fong L, Stanford KI, Gonzales JC, Yeh E, Young SG, Bensadoun A, Witztum JL, Esko JD & Moulton KS (2010). Deletion of the basement membrane heparan sulfate proteoglycan type XVIII collagen causes hypertriglyceridemia in mice and humans. *PLoS One* **5**, e13919.

Brendle C, Werner MK, Schmadl M, la Fougere C, Nikolaou K, Stefan N & Pfannenberg C (2018). Correlation of brown adipose tissue with other body fat compartments and patient characteristics: a retrospective analysis in a large patient cohort using PET/CT. *Acad Radiol* **25**, 102–110.

Caglayan AO, Baranoski JF, Aktar F, Han W, Tuysuz B, Guzel A, Guclu B, Kaymakcalan H, Aktekin B, Akgumus GT, Murray PB, Erson-Omay EZ, Caglar C, Bakircioglu M, Sakalar YB, Guzel E, Demir N, Tuncer O, Senturk S, Ekici B, Minja FJ, Sestan N, Yasuno K, Bilguvar K, Caksen H & Gunel M (2014). Brain malformations associated with Knobloch syndrome—review of literature, expanding clinical spectrum, and identification of novel mutations. *Pediatr Neurol* **51**, 806–813.e8.

Cannon B & Nedergaard J (2004). Brown adipose tissue: function and physiological significance. *Physiol Rev* **84**, 277–359.

Carobbio S, Guenantin AC, Samuelson I, Bahri M & Vidal-Puig A (2019). Brown and beige fat: From molecules to physiology and pathophysiology. *Biochim Biophys Acta* **1864**, 37–50.

Chao L, Marcus-Samuels B, Mason MM, Moitra J, Vinson C, Arioglu E, Gavrilova O & Reitman ML (2000). Adipose tissue is required for the antidiabetic, but not for the hypolipidemic, effect of thiazolidinediones. *J Clin Invest* **106**, 1221–1228.

Chouchani ET, Kazak L & Spiegelman BM (2019). New advances in adaptive thermogenesis: UCP1 and beyond. *Cell Metab* **29**, 27–37.

Cortes VA, Curtis DE, Sukumaran S, Shao X, Parameswara V, Rashid S, Smith AR, Ren J, Esser V, Hammer RE, Agarwal AK, Horton JD & Garg A (2009). Molecular mechanisms of hepatic steatosis and insulin resistance in the AGPAT2-deficient mouse model of congenital generalized lipodystrophy. *Cell Metab* **9**, 165–176.

Cypess AM, Lehman S, Williams G, Tal I, Rodman D, Goldfine AB, Kuo FC, Palmer EL, Tseng YH, Doria A, Kolodny GM & Kahn CR (2009). Identification and importance of brown adipose tissue in adult humans. *N Engl J Med* **360**, 1509–1517.

Dresner A, Laurent D, Marcucci M, Griffin ME, Dufour S, Cline GW, Slezak LA, Andersen DK, Hundal RS, Rothman DL, Petersen KF & Shulman GI (1999). Effects of free fatty acids on glucose transport and IRS-1-associated phosphatidylinositol 3-kinase activity. *J Clin Invest* **103**, 253–259.

Errera FI, Canani LH, Yeh E, Kague E, Armelin-Correa LM, Suzuki OT, Tschiedel B, Silva ME, Sertie AL & Passos-Bueno MR (2008). COL18A1 is highly expressed during human adipocyte differentiation and the SNP c.1136C >T in its "frizzled" motif is associated with obesity in diabetes type 2 patients. *An Acad Bras Cienc* **80**, 167–177.

Ferré P (2004). The biology of peroxisome proliferator-activated receptors. *Diabetes* **53**, S43.

Fontana RJ & Lok AS (2002). Noninvasive monitoring of patients with chronic hepatitis C. *Hepatology* **36**, 57.

Fukai N, Eklund L, Marneros AG, Oh SP, Keene DR, Tamarkin L, Niemelä M, Ilves M, Li E, Pihlajaniemi T & Olsen BR (2002). Lack of collagen XVIII/endostatin results in eye abnormalities. *EMBO J* **21**, 1535–1544.

Gavrilova O, Haluzik M, Matsusue K, Cutson JJ, Johnson L, Dietz KR, Nicol CJ, Vinson C, Gonzalez FJ & Reitman ML (2003). Liver peroxisome proliferator-activated receptor γ contributes to hepatic steatosis, triglyceride clearance, and regulation of body fat mass. *J Biol Chem* **278**, 34268–34276.

Gray S, Wang B, Orihuela Y, Hong EG, Fisch S, Haldar S, Cline GW, Kim JK, Peroni OD, Kahn BB & Jain MK (2007). Regulation of gluconeogenesis by Kruppel-like factor 15. *Cell Metab* **5**, 305–312.

Hanson RL, Imperatore G, Bennett PH & Knowler WC (2002). Components of the "metabolic syndrome" and incidence of type 2 diabetes. *Diabetes* **51**, 3120–3127.

Heljasvaara R, Aikio M, Ruotsalainen H & Pihlajaniemi T (2017). Collagen XVIII in tissue homeostasis and dysregulation – Lessons learned from model organisms and human patients. *Matrix Biol* **57–58**, 55–75.

Huang G, Ge G, Wang D, Gopalakrishnan B, Butz DH, Colman RJ, Nagy A & Greenspan DS (2011). α3(V) collagen is critical for glucose homeostasis in mice due to effects in pancreatic islets and peripheral tissues. *J Clin Invest* **121**, 769–783.

Im SS, Kang SY, Kim SY, Kim HI, Kim JW, Kim KS & Ahn YH (2005). Glucose-stimulated upregulation of GLUT2 gene is mediated by sterol response element-binding protein-1c in the hepatocytes. *Diabetes* **54**, 1684–1691.

Im SS, Kim MY, Kwon SK, Kim TH, Bae JS, Kim H, Kim KS, Oh GT & Ahn YH (2011). Peroxisome proliferator-activated receptor α is responsible for the up-regulation of hepatic glucose-6-phosphatase gene expression in fasting and *db/db* mice. *J Biol Chem* **286**, 1157–1164.

Inoue-Murayama M, Sugimoto Y, Niimi Y & Aso H (2000). Type XVIII collagen is newly transcribed during bovine adipogenesis. *Differentiation* **65**, 281–285.

Kahn SE (2003). The relative contributions of insulin resistance and beta-cell dysfunction to the pathophysiology of Type 2 diabetes. *Diabetologia* **46**, 3–19.

Kalinovich AV, de Jong JM, Cannon B & Nedergaard J (2017). UCP1 in adipose tissues: two steps to full browning. *Biochimie* **134**, 127–137.

Kaur I, Ruskamo S, Koivunen J, Heljasvaara R, Lackman JJ, Izzi V, Petaja-Repo UE, Kursula P & Pihlajaniemi T (2018). The N-terminal domain of unknown function (DUF959) in collagen XVIII is intrinsically disordered and highly O-glycosylated. *Biochem J* **475**, 3577–3593.

Lamming DW, Ye L, Katajisto P, Goncalves MD, Saitoh M, Stevens DM, Davis JG, Salmon AB, Richardson A, Ahima RS, Guertin DA, Sabatini DM & Baur JA (2012). Rapamycin-induced insulin resistance is mediated by mTORC2 loss and uncoupled from longevity. *Science* **335**, 1638–1643.

Lin J, Wu PH, Tarr PT, Lindenberg KS, St-Pierre J, Zhang CY, Mootha VK, Jager S, Vianna CR, Reznick RM, Cui L, Manieri M, Donovan MX, Wu Z, Cooper MP, Fan MC, Rohas LM, Zavacki AM, Cinti S, Shulman GI, Lowell BB, Krainc D & Spiegelman BM (2004). Defects in adaptive energy metabolism with CNS-linked hyperactivity in PGC-1α null mice. *Cell* **119**, 121–135.

Liu X, Wang S, You Y, Meng M, Zheng Z, Dong M, Lin J, Zhao Q, Zhang C, Yuan X, Hu T, Liu L, Huang Y, Zhang L, Wang D, Zhan J, Jong Lee H, Speakman JR & Jin W (2015). Brown adipose tissue transplantation reverses obesity in Ob/Ob mice. *Endocrinology* **156**, 2461–2469.

Makela SM, Jauhiainen M, Ala-Korpela M, Metso J, Lehto TM, Savolainen MJ & Hannuksela ML (2008). HDL2 of heavy alcohol drinkers enhances cholesterol efflux from raw macrophages via phospholipid-rich HDL 2b particles. *Alcohol Clin Exp Res* **32**, 991–1000.

Mann JP & Savage DB (2019). What lipodystrophies teach us about the metabolic syndrome. *J Clin Invest* **130**, 4009–4021.

Mariman EC & Wang P (2010). Adipocyte extracellular matrix composition, dynamics and role in obesity. *Cell Mol Life Sci* **67**, 1277–1292.

Minokoshi Y, Kahn CR & Kahn BB (2003). Tissue-specific ablation of the GLUT4 glucose transporter or the insulin receptor challenges assumptions about insulin action and glucose homeostasis. *J Biol Chem* **278**, 33609–33612.

Montanari T, Poscic N & Colitti M (2017). Factors involved in white-to-brown adipose tissue conversion and in thermogenesis: a review. *Obes Rev* **18**, 495–513.

Moulton KS, Olsen BR, Sonn S, Fukai N, Zurakowski D & Zeng X (2004). Loss of collagen XVIII enhances neovascularization and vascular permeability in atherosclerosis. *Circulation* **110**, 1330–1336.

Mu W, Cheng XF, Liu Y, Lv QZ, Liu GL, Zhang JG & Li XY (2019). Potential nexus of non-alcoholic fatty liver disease and type 2 diabetes mellitus: insulin resistance between hepatic and peripheral tissues. *Front Pharmacol* **9**, 1566.

Musso O, Rehn M, Saarela J, Theret N, Lietard J, Hintikka LD, Campion JP, Pihlajaniemi T & Clement B (1998). Collagen XVIII is localized in sinusoids and basement membrane zones and expressed by hepatocytes and activated stellate cells in fibrotic human liver. *Hepatology* **28**, 98–107.

Nakamura T, Arduini A, Baccaro B, Furuhashi M & Hotamisligil GS (2014). Small-molecule inhibitors of PKR improve glucose homeostasis in obese diabetic mice. *Diabetes* **63**, 526–534.

Nedergaard J, Wang Y & Cannon B (2019). Cell proliferation and apoptosis inhibition: essential processes for recruitment of the full thermogenic capacity of brown adipose tissue. *Biochim Biophys Acta* **1864**, 51–58.

Parhofer KG (2015). Interaction between glucose and lipid metabolism: more than diabetic dyslipidemia. *Diabetes Metab J* **39**, 353–362.

Peloso GM, Auer PL, Bis JC, Voorman A, Morrison AC, Stitziel NO, Brody JA, Khetarpal SA, Crosby JR, Fornage M, Isaacs A, Jakobsdottir J, Feitosa MF, Davies G, Huffman JE, Manichaikul A, Davis B, Lohman K, Joon AY, Smith AV, Grove ML, Zanoni P, Redon V, Demissie S, Lawson K, Peters U, Carlson C, Jackson RD, Ryckman KK, Mackey RH, Robinson JG, Siscovick DS, Schreiner PJ, Mychaleckyj JC, Pankow JS, Hofman A, Uitterlinden AG, Harris TB, Taylor KD, Stafford JM, Reynolds LM, Marioni RE, Dehghan A, Franco OH, Patel AP, Lu Y, Hindy G, Gottesman O, Bottinger EP, Melander O, Orho-Melander M, Loos RJ, Duga S, Merlini PA, Farrall M, Goel A, Asselta R, Girelli D, Martinelli N, Shah SH, Kraus WE, Li M, Rader DJ, Reilly MP, McPherson R, Watkins H, Ardissino D, NHLBI GO Exome Sequencing Project, Zhang Q, Wang J, Tsai MY, Taylor HA, Correa A, Griswold ME, Lange LA, Starr JM, Rudan I, Eiriksdottir G, Launer LJ, Ordovas JM, Levy D, Chen YD, Reiner AP, Hayward C, Polasek O, Deary IJ, Borecki IB, Liu Y, Gudnason V, Wilson JG, van Duijn CM, Kooperberg C, Rich SS, Psaty BM, Rotter JI, O'Donnell CJ, Rice K, Boerwinkle E, Kathiresan S & Cupples LA (2014). Association of low-frequency and rare coding-sequence variants with blood lipids and coronary heart disease in 56,000 whites and blacks. *Am J Hum Genet* **94**, 223–232.

Perry RJ, Samuel VT, Petersen KF & Shulman GI (2014). The role of hepatic lipids in hepatic insulin resistance and type 2 diabetes. *Nature* **510**, 84–91.

Puigserver P, Rhee J, Donovan J, Walkey CJ, Yoon JC, Oriente F, Kitamura Y, Altomonte J, Dong H, Accili D & Spiegelman BM (2003). Insulin-regulated hepatic gluconeogenesis through FOXO1–PGC-1α interaction. *Nature* **423**, 550–555.

Rachek LI (2014). Free fatty acids and skeletal muscle insulin resistance. *Prog Mol Biol Transl Sci* **121**, 267–292.

Rehn M & Pihlajaniemi T (1995). Identification of three N-terminal ends of type XVIII collagen chains and tissue-specific differences in the expression of the corresponding transcripts. The longest form contains a novel motif homologous to rat and *Drosophila* frizzled proteins. *J Biol Chem* **270**, 4705–4711.

Rodgers JT, Lerin C, Haas W, Gygi SP, Spiegelman BM & Puigserver P (2005). Nutrient control of glucose homeostasis through a complex of PGC-1α and SIRT1. *Nature* **434**, 113–118.

Rosen EJ & Xu Z (2009). Transcriptional targets in adipocyte biology. *Expert Opin Ther Targets* **13**, 975–986.

Rosen & Spiegelman BM (2006). Adipocytes as regulators of energy balance and glucose homeostasis. *Nature* **444**, 847–853.

Saarela J, Rehn M, Oikarinen A, Autio-Harmainen H & Pihlajaniemi T (1998). The short and long forms of type XVIII collagen show clear tissue specificities in their expression and location in basement membrane zones in humans. *Am J Pathol* **153**, 611–626.

Seale P, Kajimura S, Yang W, Chin S, Rohas LM, Uldry M, Tavernier G, Langin D & Spiegelman BM (2007). Transcriptional control of brown fat determination by PRDM16. *Cell Metab* **6**, 38–54.

Shepherd PR & Kahn BB (1999). Glucose transporters and insulin action—implications for insulin resistance and diabetes mellitus. *N Engl J Med* **341**, 248–257.

Shin H, Ma Y, Chanturiya T, Cao Q, Wang Y, Kadegowda AKG, Jackson R, Rumore D, Xue B, Shi H, Gavrilova O & Yu L (2017). Lipolysis in brown adipocytes is not essential for cold-induced thermogenesis in mice. *Cell Metabolism* **26**, 764–777.e5.

Takashima M, Ogawa W, Hayashi K, Inoue H, Kinoshita S, Okamoto Y, Sakaue H, Wataoka Y, Emi A, Senga Y, Matsuki Y, Watanabe E, Hiramatsu R & Kasuga M (2010). Role of KLF15 in regulation of hepatic gluconeogenesis and metformin action. *Diabetes* **59**, 1608–1615.

Tripathy D, Eriksson KF, Orho-Melander M, Fredriksson J, Ahlqvist G & Groop L (2004). Parallel manifestation of insulin resistance and beta cell decompensation is compatible with a common defect in Type 2 diabetes. *Diabetologia* **47**, 782–793.

van der Lans, Hoeks J, Brans B, Vijgen GH, Visser MG, Vosselman MJ, Hansen J, Jorgensen JA, Wu J, Mottaghy FM, Schrauwen P & van Marken Lichtenbelt WD (2013). Cold acclimation recruits human brown fat and increases nonshivering thermogenesis. *J Clin Invest* **123**, 3395–3403.

Wang F, Mullican SE, DiSpirito JR, Peed LC & Lazar MA (2013). Lipoatrophy and severe metabolic disturbance in mice with fat-specific deletion of PPARγ. *Proc Natl Acad Sci U S A* **110**, 18656–18661.

Weir JB (1949). New methods for calculating metabolic rate with special reference to protein metabolism. *J Physiol* **109**, 1–9.

Williams AS, Kang L & Wasserman DH (2015). The extracellular matrix and insulin resistance. *Trends Endocrinol Metab* **26**, 357–366.

Wilson PW, D'Agostino RB, Parise H, Sullivan L & Meigs JB (2005). Metabolic syndrome as a precursor of cardiovascular disease and type 2 diabetes mellitus. *Circulation* **112**, 3066–3072.

World Health Organization (2017). Global Health Observatory (GHO) data. http://www.who.int/gho/ncd/risk_factors/overweight_obesity/obesity_adults/en/

Xu H, Barnes GT, Yang Q, Tan G, Yang D, Chou CJ, Sole J, Nichols A, Ross JS, Tartaglia LA & Chen H (2003). Chronic inflammation in fat plays a crucial role in the development of obesity-related insulin resistance. *J Clin Invest* **112**, 1821–1830.

Yoon JC, Puigserver P, Chen G, Donovan J, Wu Z, Rhee J, Adelmant G, Stafford J, Kahn CR, Granner DK, Newgard CB & Spiegelman BM (2001). Control of hepatic gluconeogenesis through the transcriptional coactivator PGC-1. *Nature* **413**, 131–138.

Additional information

Data availability statement

The data that support the findings of this study are available from the corresponding author upon reasonable request.

Competing interests

The authors declare that there are no conflicts of interest.

Author contributions

All mouse experiments were performed at the Faculty of Biochemistry and Molecular Medicine, at the Faculty of Medicine, and at the Laboratory Animal Centre, University of Oulu. Murine blood samples were analysed at the NordLab (Oulu University Hospital, Oulu, Finland) and ultrastructural tissue analyses were conducted at the Biocenter Oulu Electron Microscopy Laboratory, University of Oulu. T.Pe., D.V., M.A., J.K., R.H. and T.Pi. contributed to conception and design of the work; T.Pe., D.V., V.I., M.A.F., K.M., I.M., M.A., J.K., S.M.K., R.D., J.T. and K.H.H. contributed to the acquisition, analysis or interpretation of data for the work. T.Pe., D.V., K.M., M.A.F., V.I., I.M., M.A., J.K., S.M.K., R.D., J.T., K.H.H., R.H. and T.Pi. all contributed to drafting or critical revision of the work. All authors approved the final version of the manuscript and agree to be accountable for all aspects of the work in ensuring that questions related to the accuracy or integrity of any part of the work are appropriately investigated and resolved. All persons designated as authors qualify for authorship, and all those who qualify for authorship are listed.

Supporting information

Additional supporting information may be found online in the Supporting Information section at the end of the article.

Statistical Summary Document